The Impact of Diamond Grind Pavement Resurfacing on PM_{10} Emissions

SPR-775
May 2024

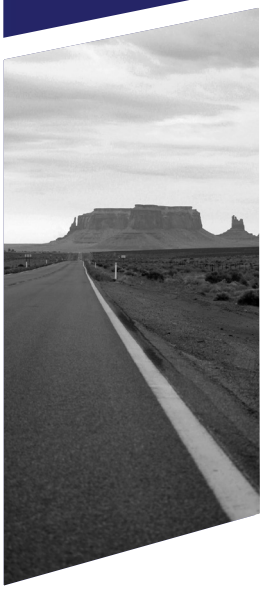

18-386

ADOT Arizona Department of Transportation Research Center

The Impact of Diamond Grind Pavement Resurfacing on PM_{10} Emissions

SPR-775

May 2024

Published by:
Arizona Department of Transportation
206 South 17th Avenue
Phoenix, Arizona 85007

In cooperation with
U.S. Department of Transportation
Federal Highway Administration

Disclaimer

This report was funded in part by the Federal Highway Administration, U.S. Department of Transportation. The contents of this report reflect the views of the authors, who are responsible for the facts and the accuracy of the data and for the use or adaptation of previously published material presented herein. The contents of this report do not necessarily reflect the official views or policies of the Arizona Department of Transportation or the Federal Highway Administration, U.S. Department of Transportation. This report does not constitute a standard, specification, or regulation. Trade or manufacturers' names that may appear herein are cited only because they are considered essential to the objectives of the report. The U.S. government and the State of Arizona do not endorse products or manufacturers.

This report is subject to the provisions of 23 USC § 407. Any intentional or inadvertent release of this material, or any data derived from its use, does not constitute a waiver of privilege pursuant to 23 USC § 407, which reads as follows:

> **23 USC § 407 — Discovery and admission as evidence of certain reports and surveys**
> Notwithstanding any other provision of law, reports, surveys, schedules, lists, or data compiled or collected for the purpose of identifying, evaluating, or planning the safety enhancement of potential accident sites, hazardous roadway conditions, or railway-highway crossings, pursuant to sections 130, 144, and 148 of this title or for the purpose of developing any highway safety construction improvement project which may be implemented utilizing Federal-aid highway funds shall not be subject to discovery or admitted into evidence in a Federal or State court proceeding or considered for other purposes in any action for damages arising from any occurrence at a location mentioned or addressed in such reports, surveys, schedules, lists, or data.

This study was conducted in accordance with Title VI of the Civil Rights Act of 1964 (78 Stat. 252.42 U.S.C. §2000d-4), Americans with Disabilities Act of 1990, and other nondiscrimination laws and authorities.

Technical Report Documentation Page

1. Report No.	2. Government Accession No.	3. Recipient's Catalog No.
SPR 000-1(023) 775	none	none

4. Title and Subtitle	5. Report Date
The Impact of Diamond Grind Pavement Resurfacing on PM_{10} Emissions	May 2024
	6. Performing Organization Code: none

7. Authors	8. Performing Organization Report No.
Jason Miech, https://orcid.org/0000-0002-0356-5088 Saed Aker, https://orcid.org/0000-0003-4071-4502 Matthew Fraser, https://orcid.org/0000-0002-6239-9104 Pierre Herckes, https://orcid.org/0000-0002-0205-3187 Kamil E. Kaloush, https://orcid.org/0000-0003-4112-0503 Jose Medina Campillo, https://orcid.org/0009-0000-3444-5276 Hasan Ozer, https://orcid.org/0000-0003-1526-6840 Michael Grandy, https://orcid.org/0009-0008-2664-2470	none

9. Performing Organization Name and Address	10. Work Unit No.
Arizona State University Office for Research and Sponsored Projects Administration Tempe, Arizona 85287-5303	none
	11. Contract or Grant No.

12. Sponsoring Agency Name and Address	13. Type of Report & Period Covered
Arizona Department of Transportation 206 S. 17th Avenue Phoenix, AZ 85007	Final Report
	14. Sponsoring Agency Code: none

15. Supplementary Notes

Prepared in cooperation with the U.S. Department of Transportation, Federal Highway Administration

16. Abstract

An assessment of tire-wear emissions was conducted to identify differences due to diamond ground and asphalt rubber asphalt concrete friction surfaces. The evaluation involved collecting representative aerosol samples from local freeways with both surface types under different meteorological conditions and with varying traffic conditions. The field study included 18 different measurement sample collections conducted at 12 sites. The amount of particulate matter was quantified using a thorough laboratory characterization process. No significant differences were observed in tire-wear emissions in the two studied surface types. The emissions at the sampling sites were also simulated using the Environmental Protection Agency's Motor Vehicle Emission Simulator software. The experimentally determined emission factors for both surfaces were in the same range as those estimated for asphalt rubber asphalt concrete friction in the previous study conducted by the Arizona Department of Transportation, but significantly lower than the model's simulated results.

17. Key Words	18. Distribution Statement	23. Registrant's Seal
Diamond Grinding, Asphalt Rubber, Particulate Matter, Tire Wear, Pavements	Document is available to the U.S. public through the National Technical Information Service, Springfield, Virginia 22161	

19. Security Classification	20. Security Classification	21. No. of Pages	22. Price
Unclassified	Unclassified	69	none

Table of Contents

Introduction **1**
Background 1
Objectives 5
Recommendations **6**
Findings **7**
Site Selection 7
Traffic *7*
Pavement Condition *9*
Site-specific Details *11*
Field Sampling Summary 11
Traffic Data Collection During Sampling 15
Traffic Volume *15*
Traffic Composition *18*
Meteorological Conditions During Sampling 20
Temperature *20*
Wind *22*
Relative Humidity *23*
Gravimetric PM_{10} Concentrations 24
Tire Markers 24
Measured Emission Factors 25
Comparison Between DG and AR-ACFC TW Emissions *27*
MOVES Simulated EF 28
Methods **32**
Overview 32
Field Sampling 32
Site Selection *32*
TW PM_{10} Sampling *34*
Used-tire Sample Collection and Processing *37*
Laboratory Characterization 38
Tire Markers Identification *38*
Gravimetric PM_{10} Concentrations *39*
Sr From Flares *39*
Emission Rate Calculation and Verification 39

Emission Modeling 39
Data Collection and Preparation *41*
Acknowledgments **43**
References **44**
Appendix A Literature Review on Tire-wear Particulate Matter Emissions **51**
Introduction 51
Factors Affecting the Generation and Particle Distribution of Tire Wear 52
Influence of Pavement Surface *52*
Vehicle Characteristics *54*
Traffic Pattern *55*
Tire-wear Markers 56
Tire-wear Components (Tire Composition) *56*
Criteria for Ideal Tire-wear Marker *57*
Rubber as a Tire-wear Marker *58*
Benzothiazoles as Tire-wear Markers *58*
Other Potential Tire-wear Markers *59*
Tire-wear Chemical Analyses 60
Mass Spectrometry *60*
Inductively Coupled Plasma Mass Spectrometry *60*
High Pressure Liquid Chromatography–Mass Spectrometry *60*
Gas Chromatography–Mass Spectrometry *61*
Gas Chromatography *62*
Miscellaneous Other Methods *62*

List of Figures

Figure 1. An Overview of Rubberized Asphalt Surface 2
Figure 2. An Overview of a Pavement Surface after Diamond Grinding 2
Figure 3. An Overview of N 64th Street Sampling Site 7
Figure 4. An Overview of Longmore Drive Sampling Site 7
Figure 5. AADT at the Selected Sites Based on 2021 Data 8
Figure 6. Traffic-Composition Categories for the Selected Candidate Sites 9
Figure 7. IRI Measurements and Classifications for the Selected Sites 10
Figure 8. Sampling Sites 13
Figure 9. Typical Sampling Operations: Overpass 14
Figure 10. Typical Sampling Operations: DG Sampling 14
Figure 11. Typical Sampling Operations: HOV Closure 14
Figure 12. Typical Sampling Operations: AR-ACFC Sampling 15
Figure 13. Typical Sampling Operations: Meteorological Conditions 15
Figure 14. Typical Sampling Operations: Traffic Counts 15
Figure 15. Traffic Volumes During Both Sampling Campaigns 17
Figure 16. Traffic Composition During Summer Sampling 18
Figure 17. Traffic Composition During Winter Sampling 19
Figure 18. Average Ambient Temperature During Sampling 20
Figure 19. Average Pavement Surface Temperature During Sampling 21
Figure 20. Average Wind Speed During Sampling 22
Figure 21. Average RH During Sampling 23
Figure 22. Gravimetric PM_{10} Concentrations Versus Vehicle Counts for AR-ACFC and DG Sites, Excluding Sweetwater Ave Summer Samples Due to Anomalous Measurements 24
Figure 23. Histogram of 2-phenylbenzothiazole Compositions for LDV and HDV Tires 25
Figure 24. Histogram of TW EFs for AR-ACFC Surfaces Versus DG Surfaces 27
Figure 25. Histogram of TW EFs for Winter Samples Versus Summer Samples 28
Figure 26. MOVES Simulated TW EFs for the Summer Sampling Sites 29
Figure 27. MOVES Simulated TW EFs for the Winter Sampling Sites 29
Figure 28. Difference in Simulated EF for the Summer and Winter Sampling Campaigns 30
Figure 29. Ratio Between Simulated and Measured TW Emissions 31
Figure 30. TW Emissions Measurement Methodology 32
Figure 31. Setting Up Traffic Control at the Victory Drive Site and Traffic Counters Installed on a Pole 33
Figure 32. Setting Up Traffic Control at the Victory Drive Site and Traffic Counters Installed on a Pole 34

Figure 33. Schematic of the Sampling Setup—
Four Flares Were Placed at Each Red Marker, Placed 50 ft Apart 35
Figure 34. Burning Flares in the HOV Lane During Sampling 35
Figure 35. Sampling Operation at Galveston Rd. Pedestrian Overpass 36
Figure 36. Overview of Rose Garden Site 36
Figure 37. Tire Source and Manufacturer Collected from CRM of America, LLC 37
Figure 38. GC–MS Device 38
Figure 39. MOVES Structure (Adapted from Kang (2013)) 40
Figure 40. EPA MOVES TW Emissions Model 40
Figure 41. MOVES Simulation for the Generated Amount of TW Emissions with Variable Speed 41
Figure 42. Vehicle Age Distribution 42
Figure 43. VTI Road Simulator (Gustafsson et al. 2012) 52
Figure 44. Relationship Between Vehicle Weight and Tire Wear (Beddows and Harrison 2021) 54
Figure 45. Camber Angle in a Vehicle Suspension System (Goodarzi and Khajepour 2017) 55
Figure 46. Toe Angle in a Vehicle Suspension System (Goodarzi and Khajepour 2017) 55

List of Tables

Table 1. Literature-Reported TW-Emission Factors (EFs) 3
Table 2. Selected Pavement Age since Surface Installation 11
Table 3. AR-ACFC Summer Sampling Sites 11
Table 4. DG Summer Sampling Sites 12
Table 5. Winter Sampling Sites 12
Table 6. Traffic Counts at Sites During Summer and Winter Sampling Periods (S1: First Hour Sample, S2: Second Hour Sample) 16
Table 7. Maximum Possible TW EFs 26
Table 8. Tire Source and Manufacturer Collected from CRM of America, LLC 37
Table 9. MOVES Input Data for Project-level Analysis 41
Table 10. MOVES Classes Counterparts in FHWA Classification 42

Acronyms, Abbreviations, and Symbols

2-PB	2-phenylbenzothiazole
AADT	annual average daily traffic
ADOT	Arizona Department of Transportation
AR-ACFC	asphalt rubber asphalt concrete friction course
ASU	Arizona State University
DG	diamond ground concrete surfaces
EB	eastbound
EF	emission factor
FHWA	Federal Highway Administration
GC–MS	gas chromatography–mass spectrometry
HDV	heavy-duty vehicles
HOV	high-occupancy vehicle lane
I	Interstate
IRI	International Roughness Index
LDV	light-duty vehicles
MAG	Maricopa Association of Governments
mph	miles per hour
MOVES	Motor Vehicle Emission Simulator
NB	northbound
PCCP	portland cement concrete pavement
PM	particulate matter
PM_{10}	particulate matter with a diameter of 10 µm or less
$PM_{2.5}$	particulate matter with a diameter of 2.5 µm or less
RH	relative humidity
SB	southbound
Sr	strontium
T factor	truck factor
TW	tire wear
TWRP	tire- and road-wear particles
EPA	Environmental Protection Agency
WB	westbound

Introduction

Background

Airborne particulate matter (PM) carries serious health and environmental consequences. The United States Environmental Protection Agency (EPA) regulates the acceptable concentrations of particles smaller than 10 µm (PM_{10}) as well as those smaller than 2.5 µm ($PM_{2.5}$) because each size poses major risks to human health. The particles between 2.5 µm and 10 µm are typically referred to as coarse particles ($PM_{10–2.5}$) while those smaller than 2.5 µm are typically referred to as fine particles.

Traffic is one of the primary contributors to airborne PM emissions (Karagulian et al. 2015, Oroumiyeh et al. 2022). Transportation-related airborne PM can be attributed to exhaust or non-exhaust sources. Non-exhaust emissions mainly originate from four sources (Thorpe and Harrison 2008, Denier van der Gon et al. 2013, Grigoratos and Martini 2014, Amato et al. 2020, EPA 2020):

- **Brake-wear emissions:** Generated from the abrasion of the brake pad, rotors, or disks.
- **Tire-wear (TW) emissions:** Generated from the contact between pavement surface and tire.
- **Road-wear emissions:** Abrasion of the road surface itself when in contact with tires.
- **Road dust resuspension:** Road dust from previously deposited materials that become airborne.

Significant reductions in vehicle-exhaust-related PM emissions have been achieved over the past two decades. However, non-exhaust components have not been regulated and now constitute a larger share of total PM emissions from mobile sources. The contribution of traffic non-exhaust emissions has risen to be almost equal to that of exhaust emissions in recent years due to improved fuel efficiency, regulations and standards imposed by the EPA and other regulating organizations, and the increased percentage of electric vehicles (Oroumiyeh and Zhu 2021). Tire-wear (TW) emissions, despite only being a portion of non-exhaust emissions, can contribute up to 10 percent of the ambient PM_{10} levels (Panko et al. 2013).

The Arizona Department of Transportation (ADOT) has been using asphalt rubber asphalt concrete friction course (AR-ACFC) overlays on Phoenix's metropolitan-area freeways primarily to reduce traffic-related noise. However, a study found that TW-related PM_{10} emissions can also be reduced by using AR-ACFC rather than the existing portland cement concrete pavement surfaces (Alexandrova et al. 2007). The AR-ACFC overlays that were constructed in the early 2000s have reached or exceeded their design lives, and ADOT is considering replacing these AR-ACFC overlays with diamond-grind (DG) concrete surfaces in the next rehabilitation cycle. Examples of both surfaces are shown in Figure 1 and Figure 2. According to a Maricopa Association of Governments' (MAG) 2020 noise reduction report, while DG surfaces are anticipated to provide similar long-term noise and friction benefits, it is not known how DG surfaces will impact TW-related PM_{10} emissions (MAG 2012).

Figure 1. An Overview of Rubberized Asphalt Surface

Figure 2. An Overview of a Pavement Surface after Diamond Grinding

According to the MAG 2012 Five Percent Plan for PM_{10} for the Maricopa County Nonattainment Area, AR-ACFC overlays provide a 30–50 percent reduction of TW-related PM_{10} emissions compared to untreated concrete surfaces (MAG 2012). Even though the overall share of TW emissions compared to total on-road traffic-related emissions is relatively small, there is significant variation in the literature in estimating their contribution. The reported reduction in TW emissions when AR-ACFC is used has been a motivating factor to support ADOT's decision to use AR-ACFC overlays since 2003, in an effort to conform to local air-quality improvement strategies. Therefore, it is important to compare the alternative rehabilitation options not only on first-time construction and maintenance costs but also from a life-cycle perspective, including environmental impact categories like TW emissions. The available PM prediction models by the EPA's Motor Vehicle Emission Simulator (MOVES) are not accurate enough to capture the differences in PM emissions due to surface-type changes. TW emissions are often estimated as the quantity of mass of PM produced per unit of vehicle distance traveled.

For example, a single milligram of tire-wear and road particles emissions would be reported as 1 mg TWRP/km/veh. Table 1 underscores the range of PM_{10} emissions reported in various sources. This report summarizes the background literature review, experimental work, and computational study that was conducted to provide a systematic comparison of the effect of changing the surface type on TW-related PM_{10} emissions.

Table 1. Literature-Reported TW-Emission Factors (EFs)

Source	Study Type	EF (mg TWRP.km^{-1}.veh^{-1}) [ounce {oz} TWRP.mile^{-1}.veh^{-1}]	Remarks
Rogge et al. (1993)	Resuspended road dust / TW simulation	7.0 [3.99 x 10^{-04}]	Applied a mass-balanced model to calculated tire PM_{10} generation rates and used annual vehicle km traveled in area
Rauterberg-Wulff (1999)	Tunnel	6.1 [3.46 x 10^{-04}]	Light vehicles
Gehrig et al. (2001)	Receptor modeling	5.0 [2.82 x 10^{-04}]	Light-duty vehicles (LDV)
Abu-Allaban et al. (2003)	Chemical mass balance receptor modeling at roadside locations	13.0 [7.41 x 10^{-04}]	LDV
Boulter et al. (2004)	Tunnel study	6.0 – 9.0 [3.42 x 10^{-04} – 5.11 x 10^{-04}]	Did not size-select tire material, assumed coarse comp = fine comp
Amann et al. (2004)	Emissions inventory (model)	6.1 ± 0.04 [3.46 x 10^{-04} ± 2.12 x 10^{-06}]	LDV/ heavy-duty vehicles (HDV)
Luhana et al. (2004)	Tunnel	0 – 6.9 [0– 3.92 x 10^{-04}]	Light vehicles
Luhana et al. (2004)	Tunnel	0 – 49.7 [0 – 2.82 x 10^{-03}]	Heavy vehicles
Kupiainen et al. (2005)	Vehicle simulator	9.0 [5.11 x 10^{-04}]	-
Alexandrova et al. (2007)	Tunnel	0.354 ± 0.071 [2.01 x 10^{-05} ± 3.88 x 10^{-06}]	Based on unreported Compound #C
Alexandrova et al. (2007)	Tunnel	0.172 ± 0.034 [9.88 x 10^{-06} ± 1.76 x 10^{-06}]	Based on unreported Compound #D
Aatmeeyata et al. (2009)	Road simulator	7.0 [3.95 x 10^{-04}]	Concrete pavement

Source	Study Type	EF (mg TWRP.km^{-1}.veh^{-1}) [ounce {oz} TWRP.mile^{-1}.veh^{-1}]	Remarks
Sjödin et al. (2010)	Road simulation study	2.2 [1.25 x 10^{-04}]	Friction tires / studded tires
Lawrence et al. (2013)	Tunnel study	No contribution from TW	Due to a lack of unique chemical tracer for TW and distinguishing TW from road wear
Panko et al. (2013)	Roadside	2.4 [1.36 x 10^{-04}]	Median
Panko et al. (2013)	Roadside	2.4 [1.36 x 10^{-04}]	95th percentile
Kwak et al. (2013)	Vehicle measurements	4.0 – 7.0 [2.26 x 10^{-04} – 3.97 x 10^{-04}]	—
Amato et al. (2020)	Simulation	6.4 – 15.6 [3.63 x 10^{-04} – 8.85 x 10^{-04}]	Electric vehicles
Baensch-Baltruschat et al. (2020)	Literature	5.0 – 53.0 [2.82 x 10^{-04} – 3.01 x 10^{-03}]	—
Prenner et al. (2021)	Model	3.6 [2.05 x 10^{-04}]	—
Harrison et al. (2021)	European Monitoring and Evaluation Programme (EMEP)/European Environment Agency (EEA) emission inventory	5.8 – 8.7 [3.28 x 10^{-04} – 4.94 x 10^{-04}]	Cars
Harrison et al. (2021)	EMEP EEA emission inventory	14.0 – 20.7 [7.95 x 10^{-04} – 1.18 x 10^{-03}]	LGVs

Objectives

The goal of this research study was to compare the PM_{10} TW emissions of DG resurfacing with the emissions of AR-ACFC overlays. Specific objectives were as follows:

1. Identify the chemical components that are unique to TW particles to differentiate this emission source from other particle emissions from mobile sources.
2. Collect representative air-quality samples from local freeways with both AR-ACFC and DG surfaces to quantify TW emissions and provide a comprehensive analysis of potential differences.
3. Study the effect of spatial, meteorological, and traffic-related factors may have on TW emissions per both surface types.
4. Derive TW EF of both DG and AR-ACFC surfaces and identify any significant differences between the surfaces.
5. Compare TW field measurements to project field simulation using EPA's MOVES.

Recommendations

The study involved aerosol sampling of TW-PM emissions from 18 different measurement sample collections conducted at 12 sites. The sites were distributed equally between DG and AR-ACFC surfaces. The sampling operation was conducted in both summer and winter seasons.

Below are the major findings and takeaways for future applications and studies:

1. There was not a statistically different rate of TW-particulate matter emissions between DG and AR-ACFC pavement surfaces based on the measured gravimetric PM_{10} emissions, TW-marker concentrations, and the derived EFs.
2. TW PM_{10} EFs were lower in the winter compared to summer. This observation is consistent with the sensitivity of PM emissions to meteorological conditions, verifying the robustness of the sampling and characterization process.
3. The effect of traffic volume on the TW emissions was not distinguished precisely. A more robust correlation between the TW emissions and traffic characteristics can be established using on-vehicle measurement systems.
4. The MOVES results were within the range of values reported in the literature and were significantly higher than TW EFs measured during this field sampling campaign. While MOVES may yield adequate estimates when applied on a national or county scale, it proves ineffective for estimating TW at the project level. This is because some factors, such as seasonal effects (temperature, wind, humidity changes) and surface-type effects, cannot be captured by MOVES.
5. Certain factors that may impact emissions levels were not examined in this study but might warrant examination in the future. For instance, other non-exhaust emissions and particulate matter emitted during construction or maintenance activities could have an influence on PM_{10} emissions levels from the two surface types. Additionally, to provide a comprehensive evaluation of the integrity of the two surface types as it relates to emissions, a life-cycle assessment of the two surface treatments could be undertaken.

It is important to acknowledge the challenges and limitations of the field aerosol sampling that introduced inherent variability in the collected samples that was beyond the research team's control or monitoring capabilities. For instance, data about acceleration and braking on the highway (which have been reported to be one of the principal sources of TW emissions) were not captured in the sampling. Differences in pavement age and condition can affect texture characteristics present during the sampling. The age and condition of the pavements were not a controlled variable in the study and varied among the sites.

Findings

Site Selection

Based on the literature survey presented in Appendix A, key factors used to determine site selection for sampling sites included traffic volume, traffic composition, and pavement condition. Site selection also considered those characteristics which allowed for a safe and robust sampling operation. Figure 3 and Figure 4 illustrate an overview of the selected sites for sampling followed by a discussion on the key characteristics of the sites.

Figure 3. An Overview of N 64th Street Sampling Site

Figure 4. An Overview of Longmore Drive Sampling Site

Traffic

Traffic volume is reported to be one of the most influential factors affecting TW and resulting emissions. Annual average daily traffic (AADT) counts were obtained for all candidate sampling sites. The selected sites were divided into four categories based on the 2021 AADT data provided by ADOT: under 100,000; between 100,000 and 150,000; between 150,000 and 200,000; and above 200,000. The sites that fall into each category and their respective AADTs, as well as the projected future AADTs for the year 2040, provided by ADOT, are shown in Figure 5.

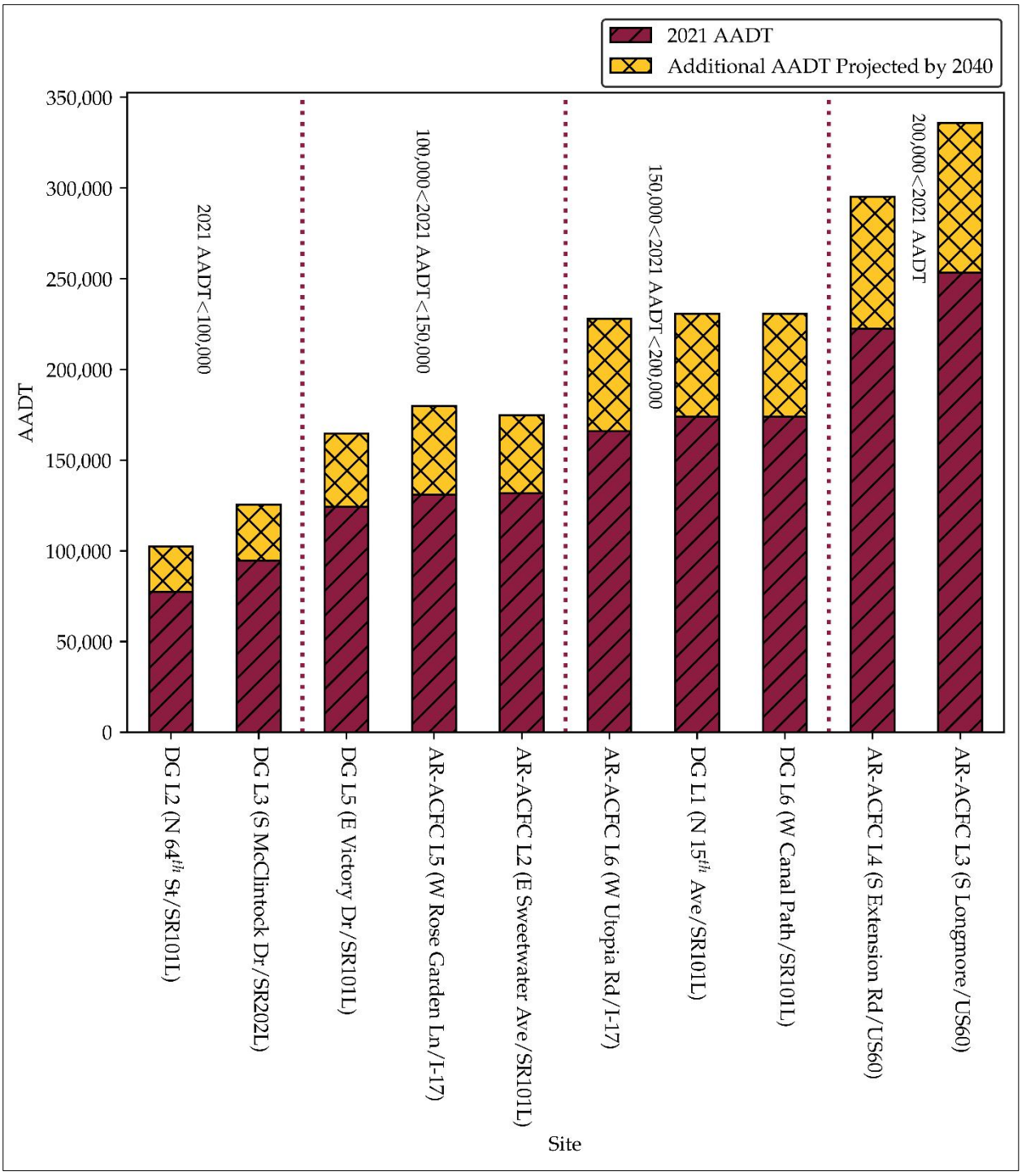

Figure 5. AADT at the Selected Sites Based on 2021 Data

The traffic composition of each site was also used to divide the potential sampling sites into three subcategories based on the truck (T) factor, which describes the percentage of the total AADT composed of single-unit and combination trucks. The three categories for traffic composition (T factor) include:

- Under 6.5 percent
- Between 6.5 percent and 7.5 percent
- Greater than 7.5 percent

Figure 6 shows the three categories and the T factor for each potential site.

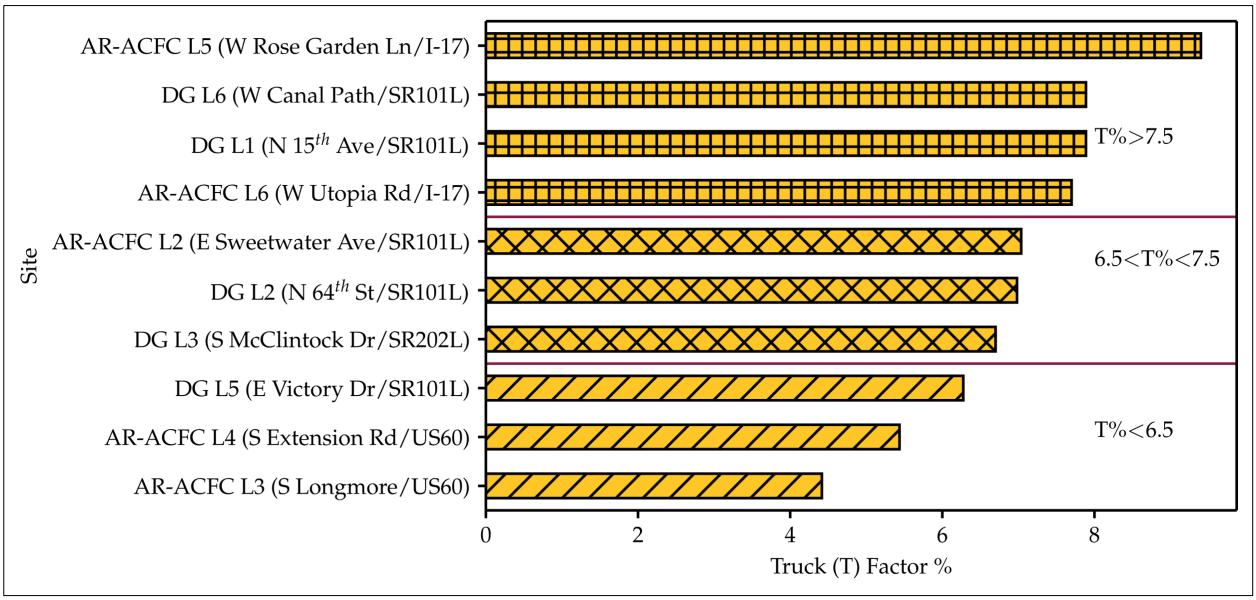

Figure 6. Traffic-Composition Categories for the Selected Candidate Sites

Pavement Condition

ADOT's transportation systems management and operations division provided the International Roughness Index (IRI), rutting data, and cracking data from 2021, of the sites where available. IRI is the only measure where a direct comparison could be made between the candidate sites. IRI, measured in inches per mile, was grouped into three subcategories:

- IRI less than 50
- Between 50 and 75
- More than 75

The IRI values for each site are presented in Figure 7.

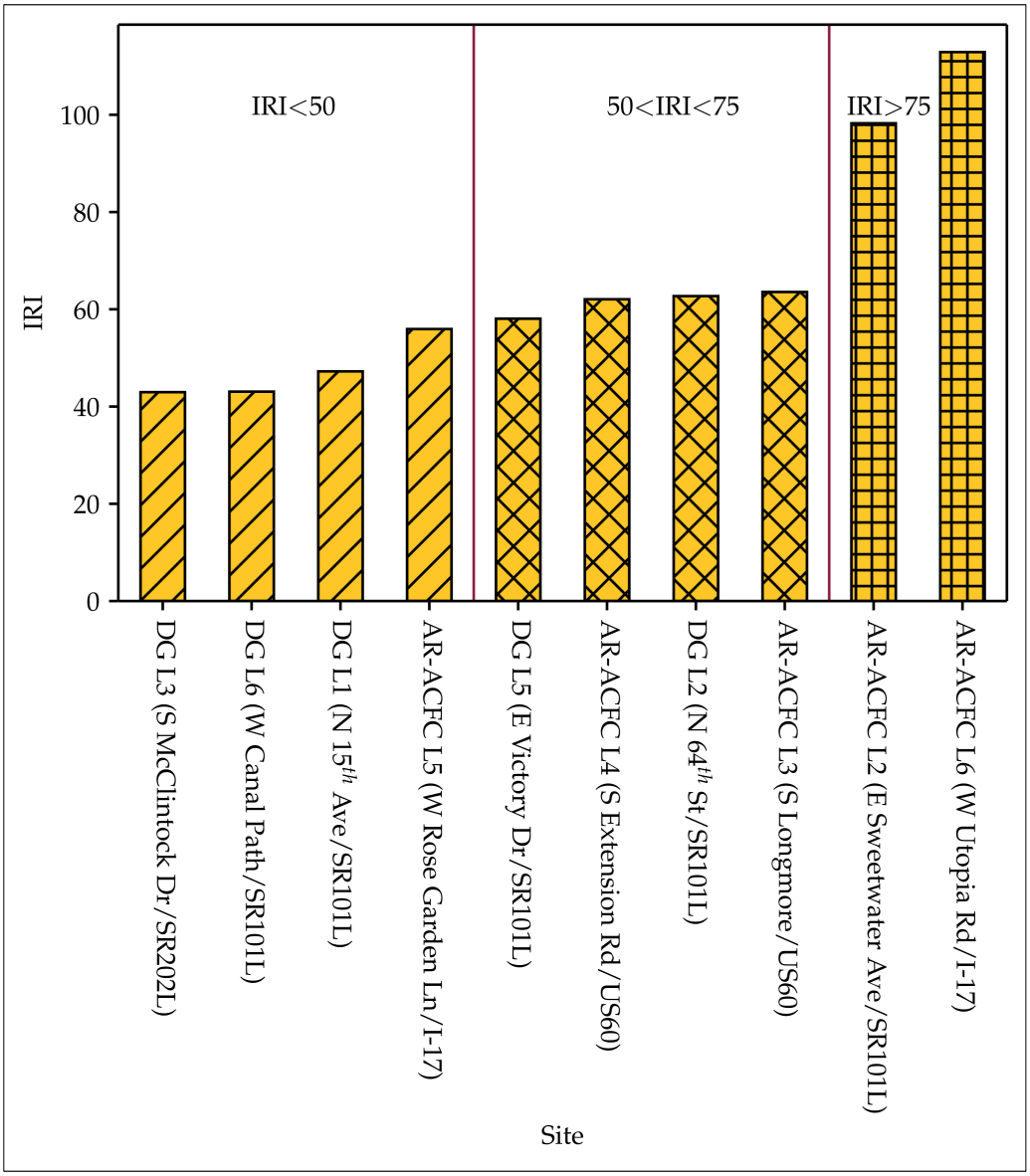

Figure 7. IRI Measurements and Classifications for the Selected Sites

Site-specific Details

Site-specific details, like the age of the pavement (presented in Table 2), the geometry of the highway (e.g., horizontal curvatures were avoided due to safety concerns for short lane closure intervals), and the distance between the overpass and the highway were considered during site selection.

Table 2. Selected Pavement Age since Surface Installation

ID	Route	Overpass	Age (years)	ID	Route	Overpass	Age (years)
L1	SR 101 Loop	E Thomas Rd	19	L1	SR 101 Loop	N 15th Ave	1
L2	SR 101 Loop	E Sweetwater Ave	19	L2	SR 101 Loop	N 64th St	1
L3	US 60	S Longmore	17	L3	US 60	S McClintock Dr	2
L4	US 60	S Extension Rd	17	L4	US 60	W Galveston St	*
L5	I-17	W Rose Garden Ln	*	L5	I-17	E Victory Dr	2
L6	I-17	W Utopia Rd	*	L6	I-17	W Canal Path	2

*Data not available.

Field Sampling Summary

Two field sampling campaigns were carried out: the first from July to October in 2022, and the second during January and February in 2023. Sampling in different seasons created the ability to account for the effect of roadway temperature on TW-emission rates. The sampling spanned across 12 sites located on four major interstate routes and state routes within Maricopa County in the Phoenix metropolitan area. The sampling was completed in close coordination with various departments of ADOT. Prior to traveling to each site, ADOT staff and the Arizona State University (ASU) research team met to organize and review the sampling plan for each site to provide a safe and efficient data collection in the work zones. Table 3, Table 4, and Table 5 present a summary of the sampling sites and the timeframes of the sampling. A map presenting the locations of the sampling sites can be found in Figure 8.

Table 3. AR-ACFC Summer Sampling Sites

ID	Route	Overpass	Sampling Location	Sampling Date	Sampling Times (AM)
L1	SR 101 Loop	E Thomas Rd	NB HOV	9/27/2022	08:51 – 11:26
L2	SR 101 Loop	E Sweetwater Ave	NB HOV	7/15/2022	08:58 – 11:54
L3	US 60	S Longmore	EB HOV	9/13/2022	08:30 – 11:06
L4	US 60	S Extension Rd	SB HOV	10/11/2022	08:54 – 11:28
L5	I-17	W Rose Garden Ln	NB HOV	8/17/2022	08:27 – 10:50
L6	I-17	W Utopia Rd	NB HOV	8/24/2022	08:29 – 10:42

Table 4. DG Summer Sampling Sites

ID	Route	Overpass	Sampling Location	Sampling Date	Sampling Time
L1	SR 101 Loop	N 15th Ave	NB HOV	8/31/2022	8:32–10:55
L2	SR 101 Loop	N 64th St	WB HOV	9/7/2022	8:39–11:11
L3	US 60	S McClintock Dr	EB HOV	9/14/2022	8:27–10:59
L4	US 60	W Galveston St	SB HOV	9/28/2022	8:36–11:13
L5	I-17	E Victory Dr	SB HOV	8/10/2022	9:14–11:35
L6	I-17	W Canal Path	SB HOV	10/12/2022	9:36–11:29

Table 5. Winter Sampling Sites

ID	Route	Overpass	Sampling Location	Sampling Date	Sampling Time
AR-ACFC L1	SR 101 Loop	E Thomas Rd	NB HOV	2/15/2023	8:38–10:41
AR-ACFC L1	SR 101 Loop	E Thomas Rd	NB HOV	2/16/2023	8:21–10:18
AR-ACFC L2	SR 101 Loop	E Sweetwater Ave	NB HOV	1/20/2023	8:44–10:45
DG L1	SR 101 Loop	N 15th Ave	WB HOV	1/18/2023	9:20–11:34
DG L2	SR 101 Loop	N 64th St	SB HOV	1/25/2023	8:35–10:43
DG L4	SR 101 Loop	W Galveston St	NB HOV	1/24/2023	8:50–10:59

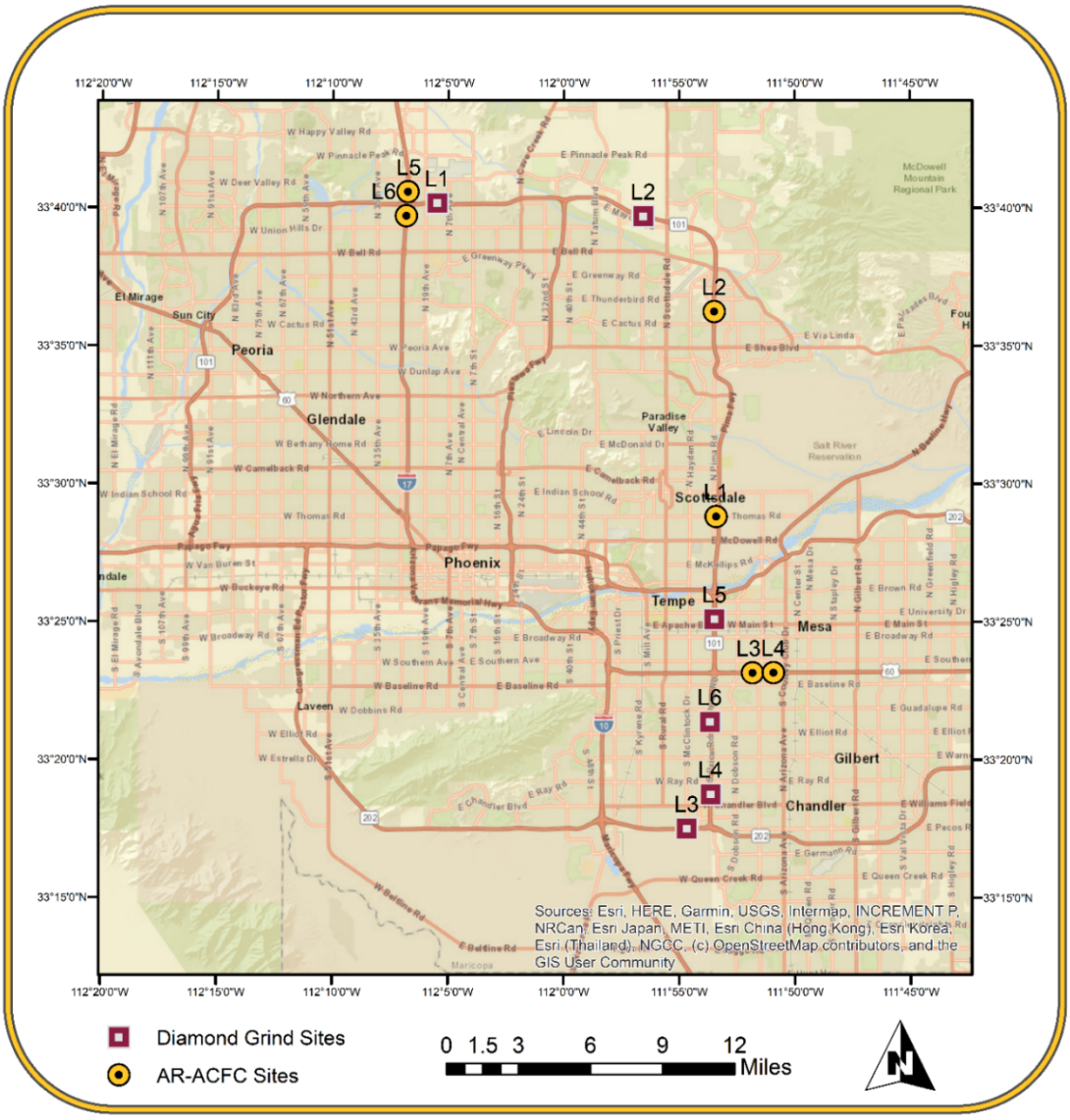

Figure 8. Sampling Sites

Figure 9, Figure 10, Figure 11, Figure 12, Figure 13, and Figure 14 present the key steps followed during the sampling operation.

Figure 9. Typical Sampling Operations: Overpass

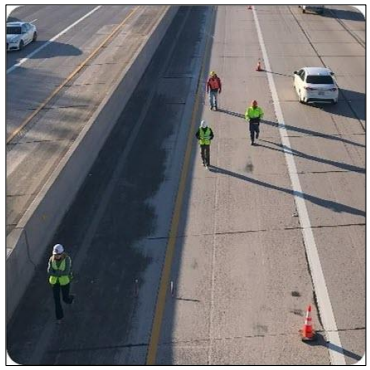

Figure 10. Typical Sampling Operations: DG Sampling

Figure 11. Typical Sampling Operations: HOV Closure

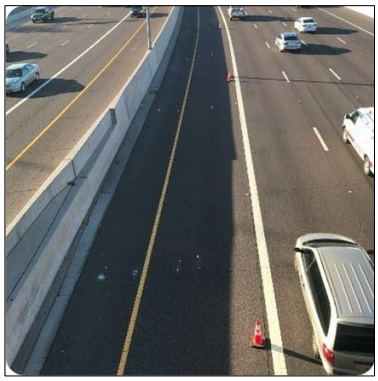

Figure 12. Typical Sampling Operations: AR-ACFC Sampling

Figure 13. Typical Sampling Operations: Meteorological Conditions

Figure 14. Typical Sampling Operations: Traffic Counts

Traffic Data Collection During Sampling

Traffic data were collected using the counters installed at each site by a vendor specialized in data collection for state and local agencies.

Traffic Volume

During the first hour of winter sampling, the overall traffic volume on the highways ranged between 9,972 and 13,542 vehicles, as shown in Table 6. Figure 15 shows the overall hourly traffic volume at all sites sampled during both summer and winter sampling. No significant difference in the overall hourly traffic volume between summer and winter sampling was found for any sites.

Table 6. Traffic Counts at Sites During Summer and Winter Sampling Periods (S1: First Hour Sample, S2: Second Hour Sample)

Site	Summer S1	Summer S2*	Winter S1	Winter S2*
AR-ACFC L1 (E Thomas Rd / SR 101L)	12,547	—	13,542	12,862
AR-ACFC L2 (E Sweetwater Ave / SR 101L)	14,644	15,166	11,022	—
AR-ACFC L3 (S Longmore / US 60)	14,330	—	—	—
AR-ACFC L4 (S Extension Rd / US 60)	14,453	—	—	—
AR-ACFC L5 (W Rose Garden Ln / I-17)	9,176	8,382	—	—
AR-ACFC L6 (W Utopia Rd / I-17)	8,348	7,303	—	—
DG L1 (N 15th Ave / SR 101L)	11,742	10,977	11,017	—
DG L2 (N 64th St / SR 101L)	11,747	9,412	11,714	—
DG L3 (S McClintock Dr / SR 202L)	6,791	—	—	—
DG L4 (W Galveston St / SR 101L)	9,573	—	9,972	—
DG L5 (E Victory Dr / SR 101L)	12,908	12,146	—	—
DG L6 (W Canal Path / SR 101L)	11,050	—	—	—

* Due to similarities of initial traffic counts in the first (S1) and second (S2) hours, traffic sampling was modified part-way through the study to only conduct one hour of traffic-count measurement.

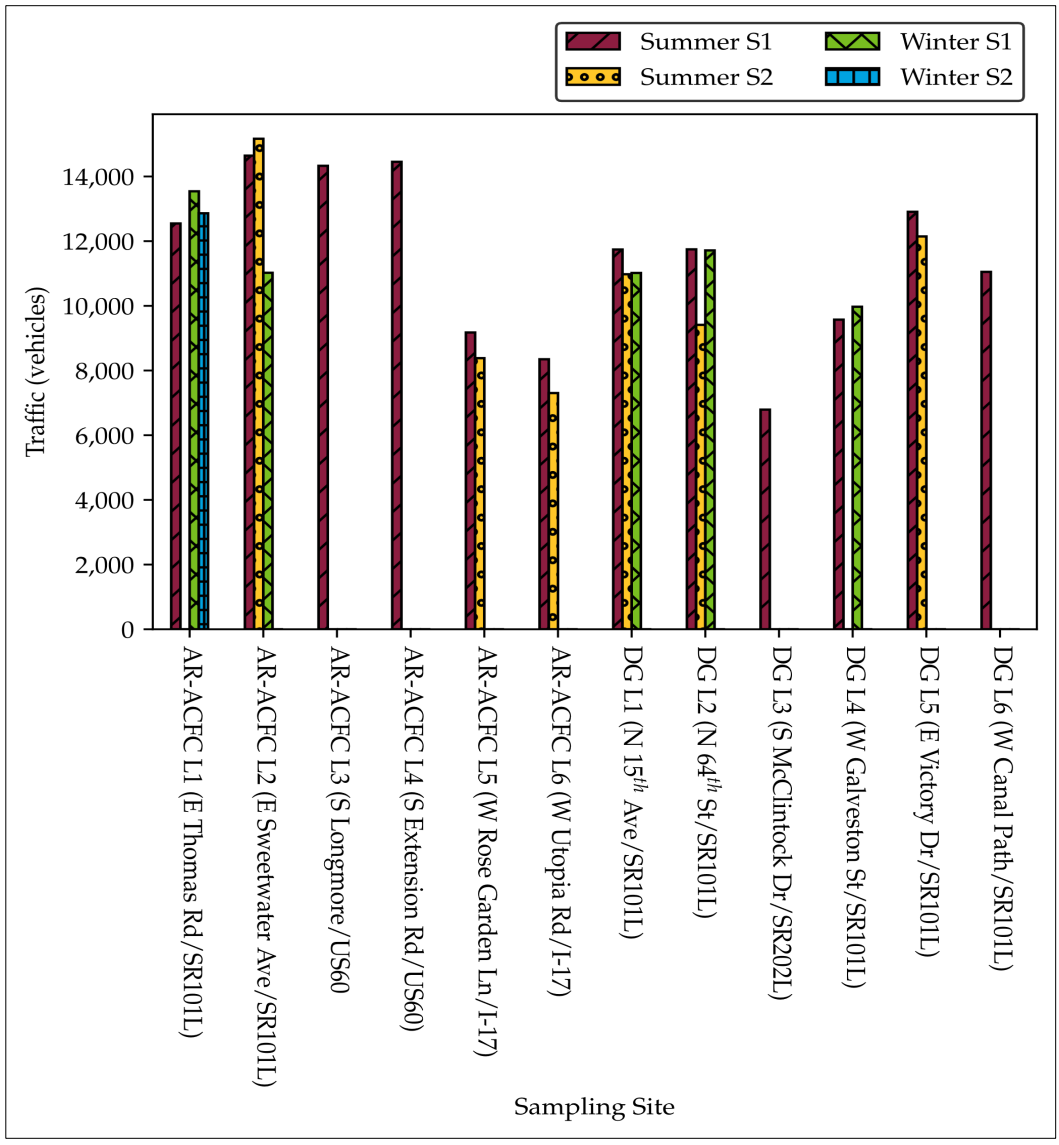

Figure 15. Traffic Volumes During Both Sampling Campaigns

Traffic Composition

The traffic-composition data were collected based on the Federal Highway Administration's (FHWA) vehicle classification system. However, in order to make the data easier to interpret, FHWA Classes 1–3, which are considered LDVs, were grouped together. The rest of the 13 classes were also grouped together, since they can be considered HDVs. Traffic compositions in both summer and winter campaigns are presented in Figure 16 and Figure 17, respectively. Data from the winter sampling campaign (as shown in Figure 17) only included five of the twelve sites where measurements were taken during the summer campaign. LDVs dominated the traffic in all sites during both sampling campaigns, as HDVs remained below 8 percent throughout sampling.

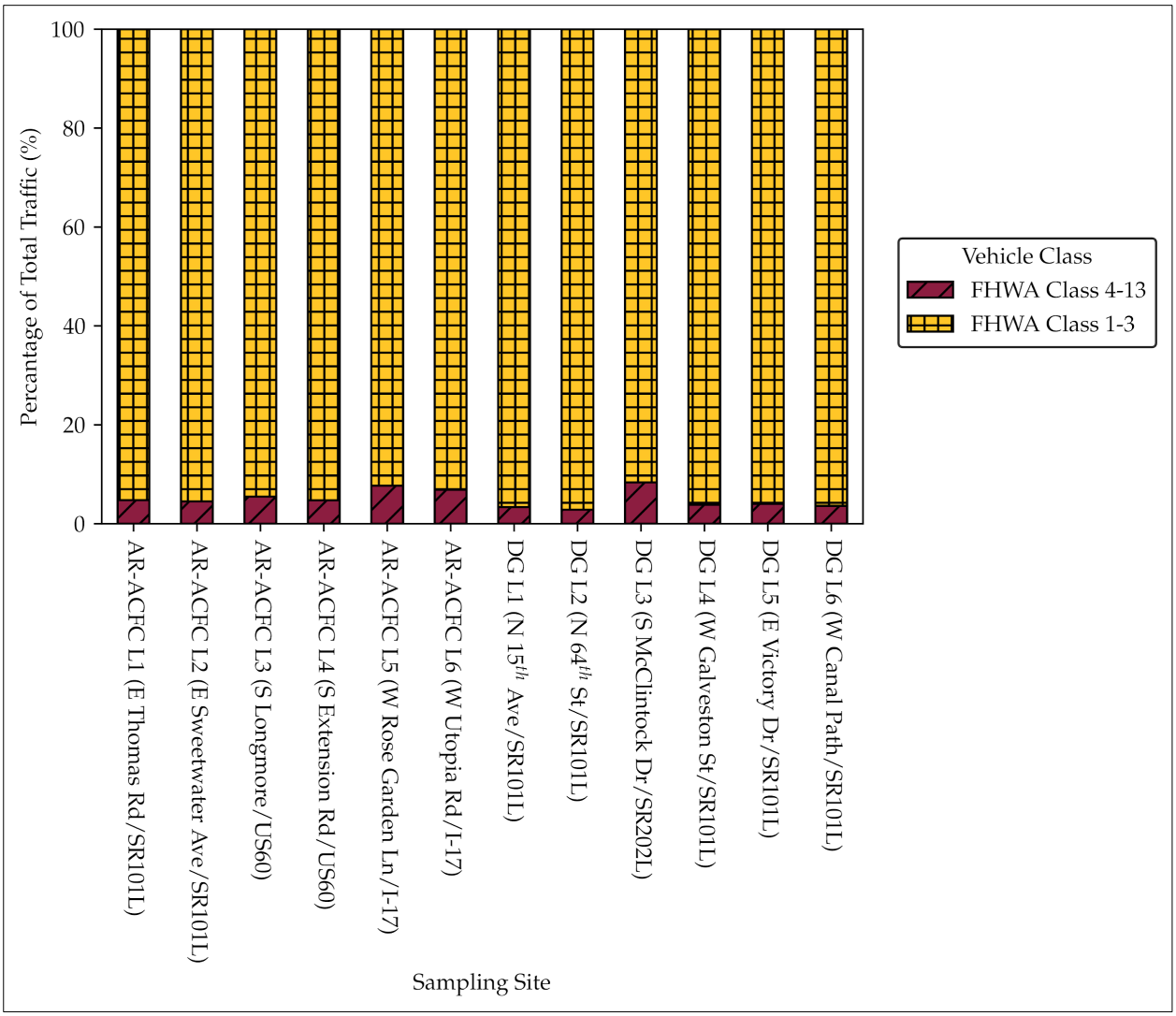

Figure 16. Traffic Composition During Summer Sampling

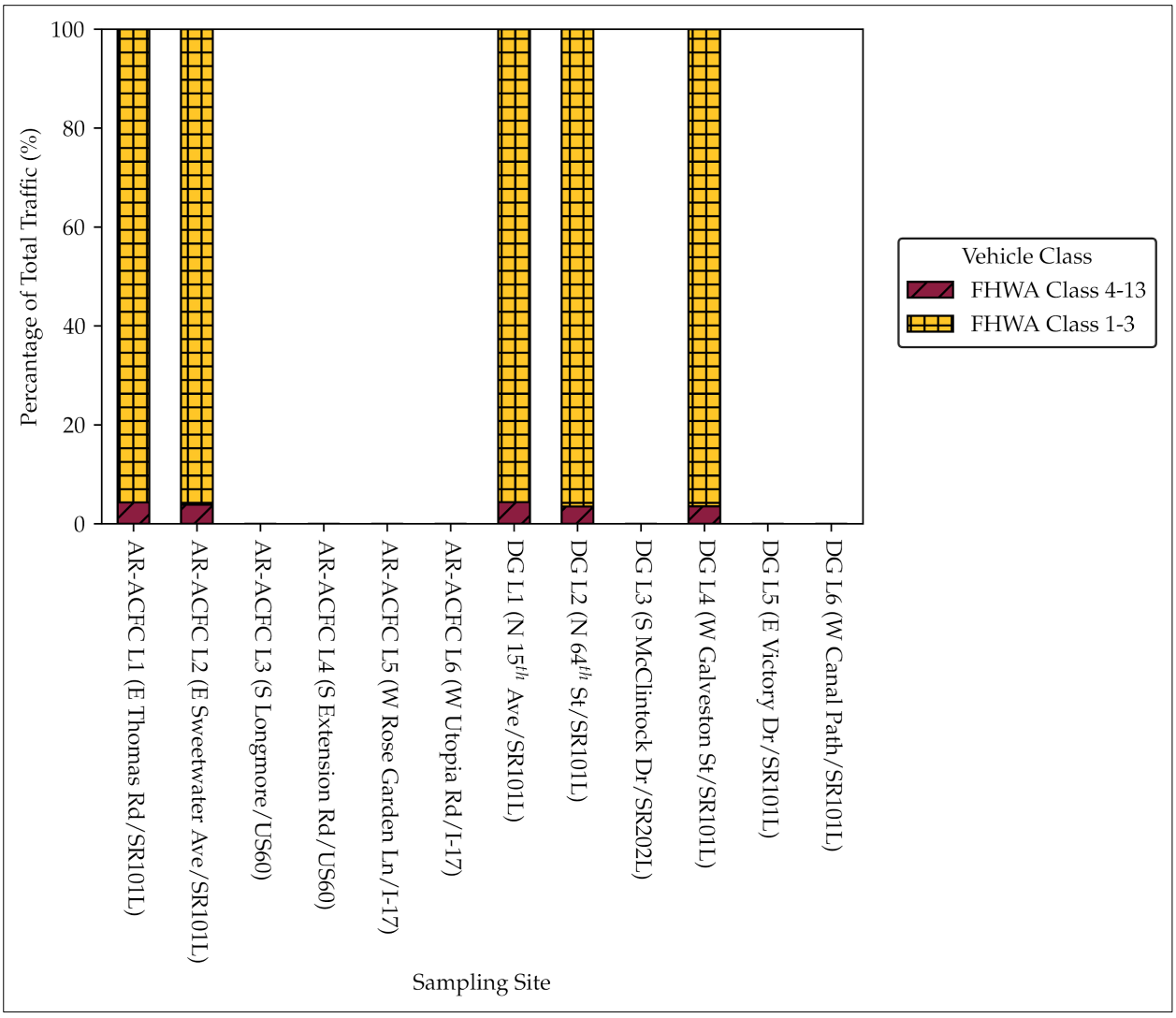

Figure 17. Traffic Composition During Winter Sampling

Meteorological Conditions During Sampling

Temperature

The ambient air temperature and pavement surface temperature were recorded during sampling, and the average temperatures are presented in Figure 18 and Figure 19, respectively. The temperature during winter sampling was roughly 30° C lower than that measured during summer sampling.

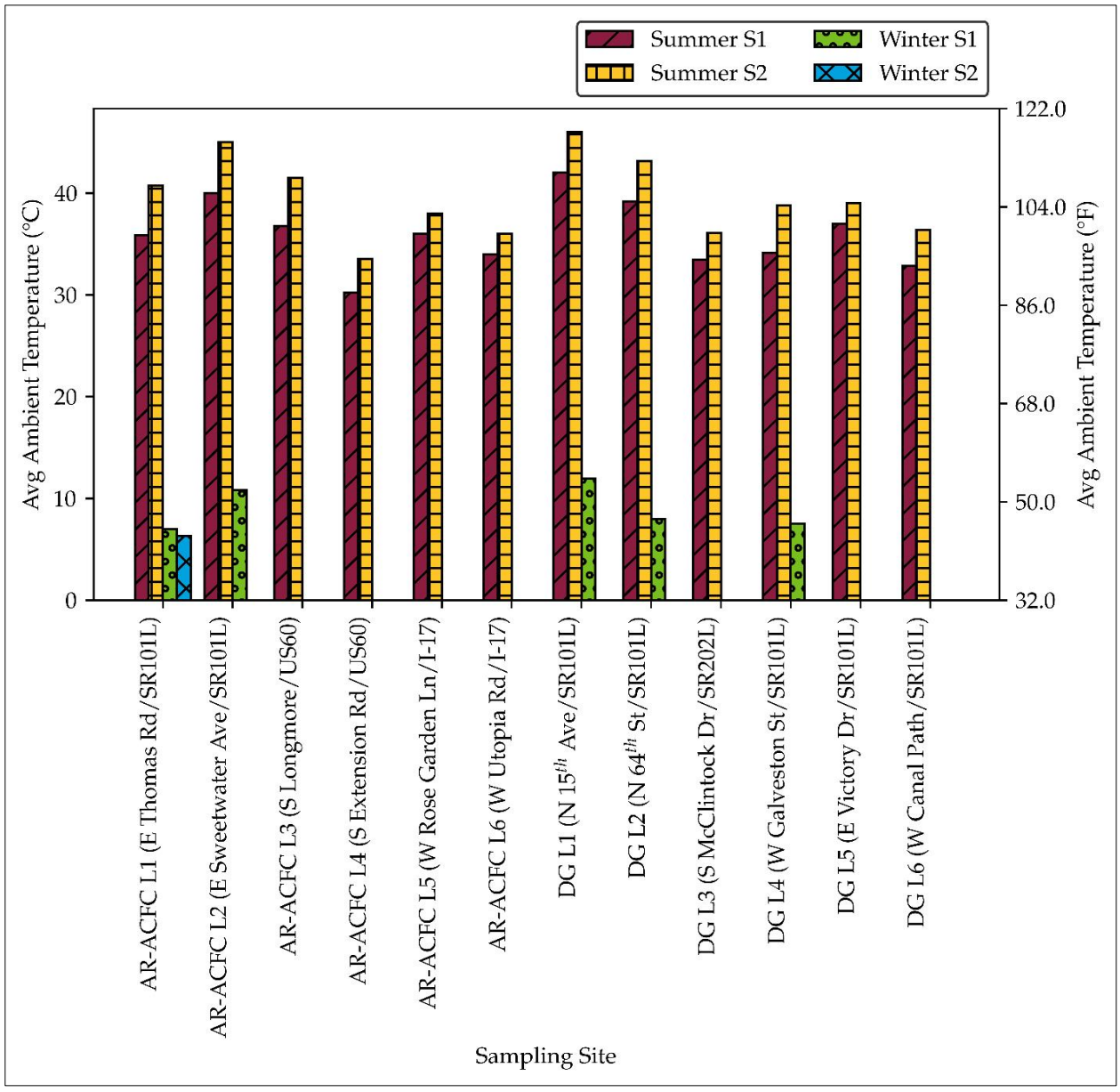

Figure 18. Average Ambient Temperature During Sampling

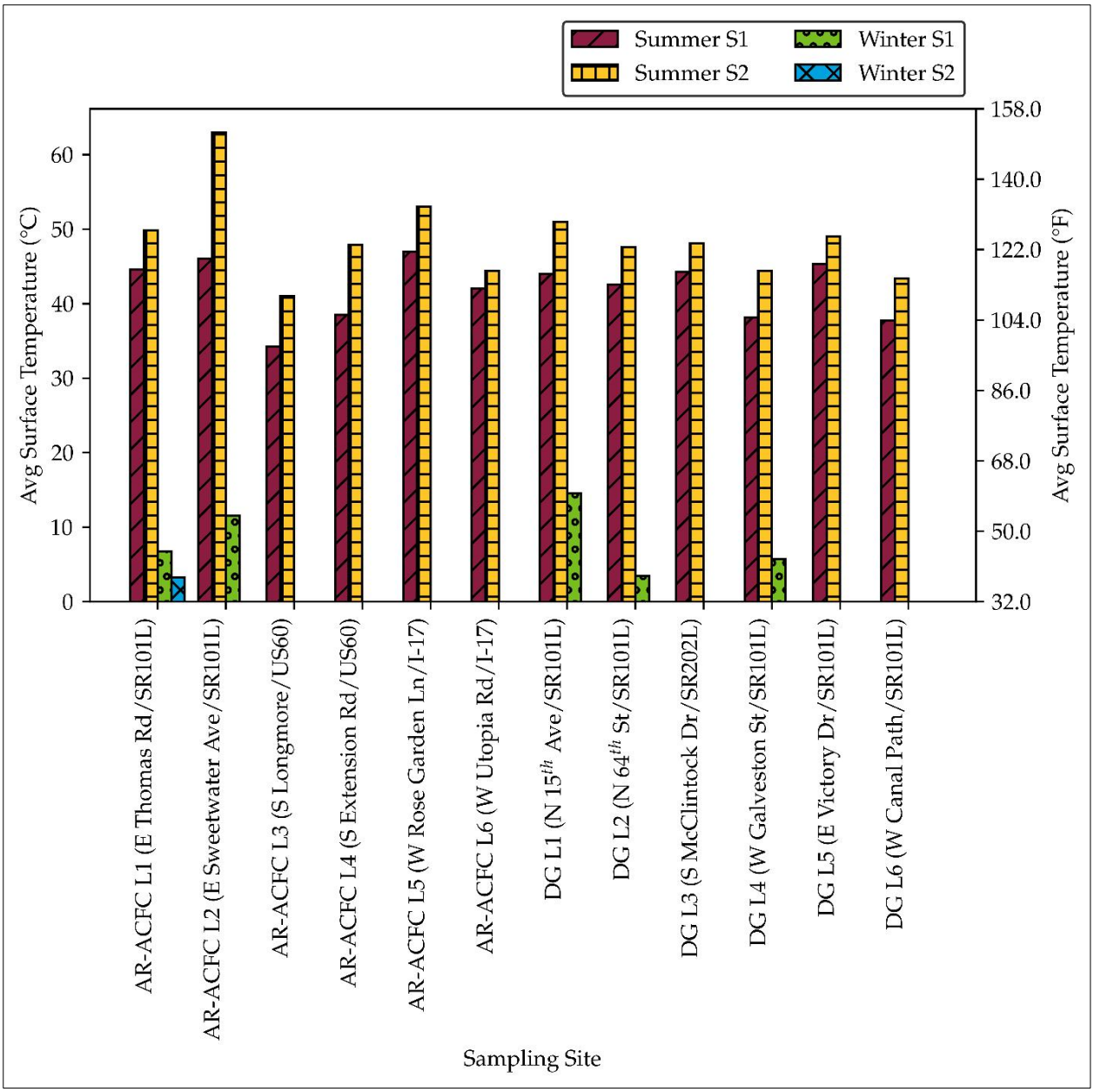

Figure 19. Average Pavement Surface Temperature During Sampling

Wind

The average wind speed during both summer and winter sampling is presented in Figure 20. The wind speed remained relatively low on average during sampling. A few exceptions were observed in the summer sampling campaign. The average wind speed did not exceed two miles per hour (mph) throughout the winter sampling campaign.

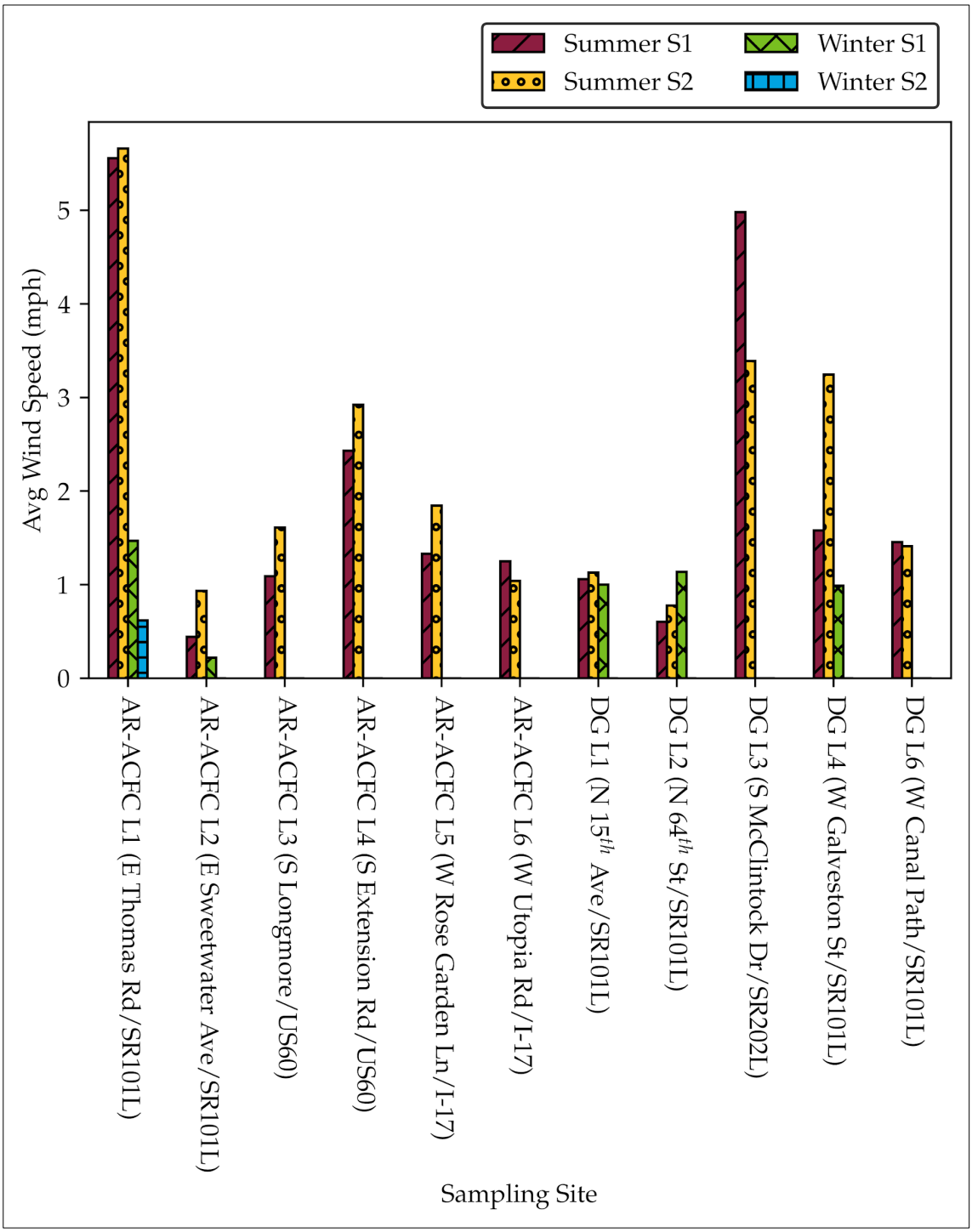

Figure 20. Average Wind Speed During Sampling

Relative Humidity

Relative humidity (RH) was measured in all locations and compared to the temperature. Lower temperature often led to higher RH, as shown in Figure 21. RH was significantly higher in the winter campaign compared to RH during the summer campaign.

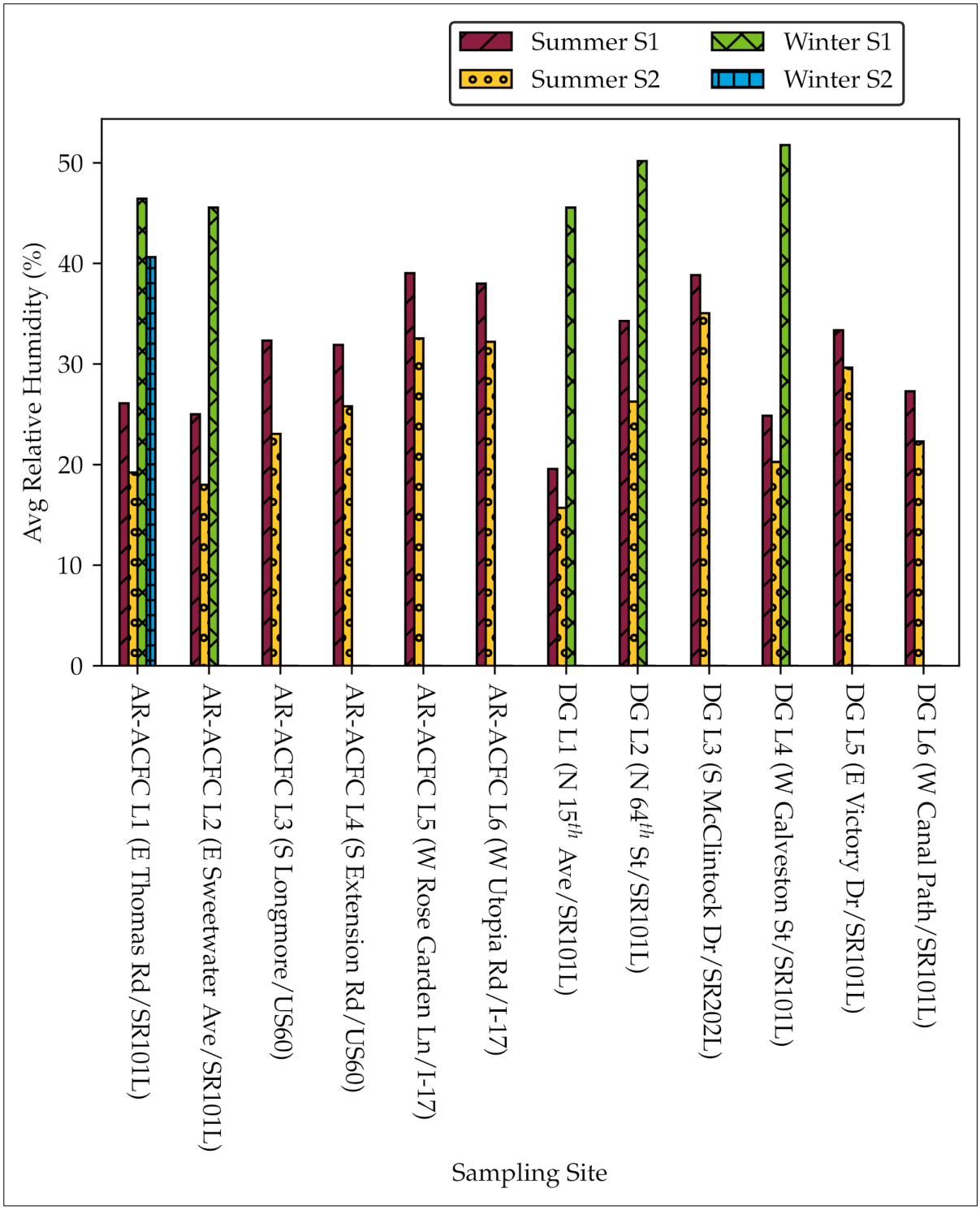

Figure 21. Average RH During Sampling

Gravimetric PM_{10} Concentrations

Contact between a tire and the pavement surface causes the tire to wear and can cause airborne particle emissions. While PM_{10} measurements were made at each site, these aggregated measurements are not solely due to TW emissions, as brake wear, resuspended road dust, and non-highway emission sources such as mineral dust all contribute to the concentration of PM_{10} measured in urban locations. Figure 22 demonstrates that there is no apparent correlation between PM_{10} concentrations and traffic counts for all sampled sites. It also shows that there is not a clear difference between the PM_{10} concentrations of different surface types, indicating non-highway-related factors may contribute to measured PM_{10} concentrations. This observation highlights the need to focus the analysis on tire-specific chemical markers rather than on measurements of total PM_{10}. An additional factor that must be considered when using ambient measurements to quantify air-pollution-source emission rates is the mixing of air from the highway surface to the overpass sampling site. This can result in variable wind speed and direction as fast-moving vehicles cause turbulence and atmospheric mixing. By using an artificial-PM tracer at the highway surface, such as a road flare, the research team was able to account for this mixing and transport effect.

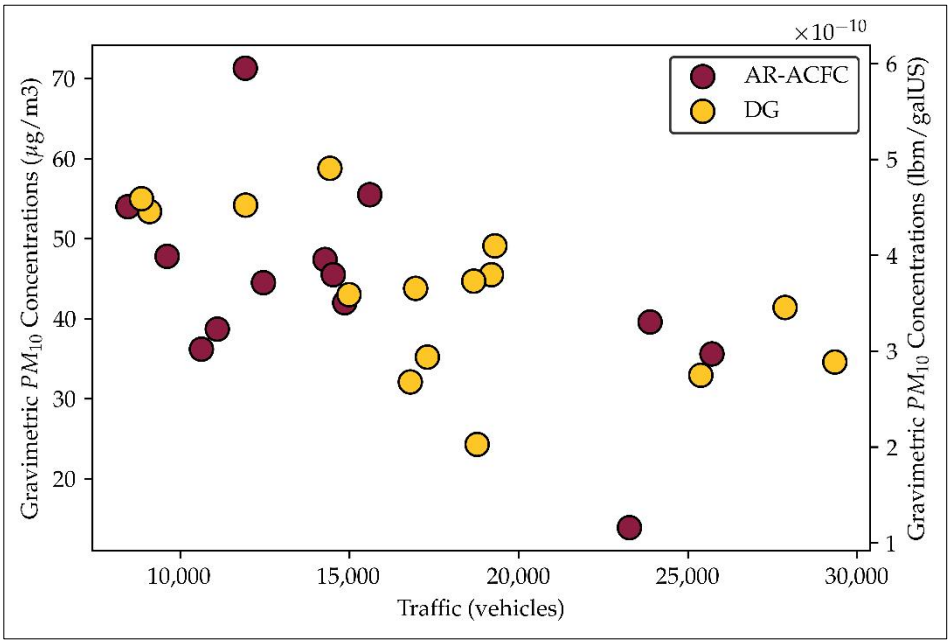

Figure 22. Gravimetric PM_{10} Concentrations Versus Vehicle Counts for AR-ACFC and DG Sites, Excluding Sweetwater Ave Summer Samples Due to Anomalous Measurements

Tire Markers

Chemical markers were developed to isolate TW from the total PM_{10} emissions. When selecting a marker to use, it is important that it be specific to the unique source of interest and present in a measurable quantity. Benzothiazoles were chosen as tire markers after a literature search identified them as vulcanization accelerators used solely in the tire-manufacturing process. Further lab testing confirmed the presence of several benzothiazoles in local tire samples, including 2-phenylbenzothiazole (2PB), N-cyclohexyl-2-benzothiazolamine, benzothiazole, and 2-hydroxybenzothiazole. However, only

2PB was quantified in this study's highway samples; therefore, it was the only marker used for the analysis. To convert highway marker concentrations into highway TW concentrations, the research team quantified the 2PB composition of 16 local tire samples. These tire samples consisted of a variety of tire brands and models with a 50:50 mix of light-duty and heavy-duty vehicle tires. Figure 23 shows the 2PB compositions of the LDVs and HDVs. On average, the HDV tires had a 2PB composition seven times higher than LDV tires. Due to this difference in tire composition, the research team calculated a weighted average 2PB composition based on the traffic-composition data (i.e., LDV and HDV percentage) at each site to properly convert from tire-marker to TW concentrations.

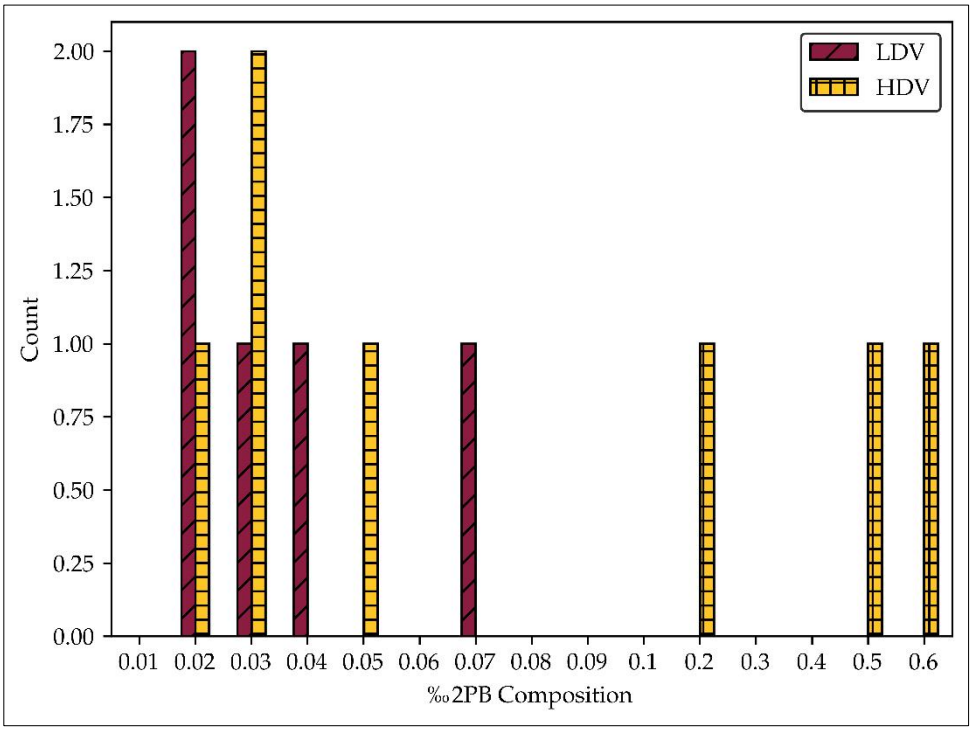

Figure 23. Histogram of 2-phenylbenzothiazole Compositions for LDV and HDV Tires

Measured Emission Factors

TW PM_{10} emission factors (EFs) were calculated for each site and are shown in Table 7. Both samples from L2 AR-ACFC were omitted due to anomalous mass measurements. Also omitted were both samples from L1 AR-ACFC due to low Strontium (Sr) recovery values, and Sample 1 from L4 DG due to an extraction error. Tire markers were not detected at several winter sites (L1.1W AR-ACFC, L1.2W AR-ACFC, L2W AR-ACFC, L2W DG, & L4W DG), so the EFs detected in those samples represent the maximum possible EF calculated from the 2PB method detection limit. The highest EFs were observed in samples at sites L6 AR-ACFC, L3 DG, and L5 DG. When inputting the same tire-marker concentration (2PB MDL of 0.029 µg/mL [3.02×10^{-8} oz/fluid ounce {fl oz}]) into calculations for these samples, the same trend was observed.

Using auxiliary data, the research team determined that the higher EF values at L3 DG were due to low Sr recovery, and the higher EFs at L6 AR-ACFC and L5 DG were due to shorter sampling times than the rest of the sites. Therefore, these differences are most likely representative of the variability within the calculations and methods used rather than any real differences between TW occurring at the sites. These EFs are an order of magnitude less than the values determined in most previous studies at other locations, such as Kupiainen et al. (2005) (8.7 mg TWRP.km^{-1}.veh^{-1} [4.94 x 10^{-04} oz TWRP.mile^{-1}.veh^{-1}]), Alves et al. (2020) (2.0 mg TWRP.km^{-1}.veh^{-1} [1.13 x10^{-04} oz TWRP.mile^{-1}.veh^{-1}]), and Hicks et al. (2021) (8.1 mg TWRP.km^{-1}.veh^{-1} [4.59 x 10^{-04} oz TWRP.mile^{-1}.veh^{-1}]).

However, Aatmeeyata et al. (2009) calculated an EF of 3.7x10^{-3} mg TWRP.km^{-1}.veh^{-1} [2.1 x10^{-7} oz TWRP.mile^{-1}.veh^{-1}] although a previous tunnel study in Phoenix, Arizona, calculated values of (0.172 – 0.354 mg TWRP.km^{-1}.veh^{-1} [9.88 x 10^{-06} – 2.01 x 10^{-05} oz TWRP.mile^{-1}.veh^{-1}]) (Alexandrova et al. 2007).

Table 7. Maximum Possible TW EFs

Site ID	Route	Overpass	Sample #	TW EFs (mg TWRP.km^{-1}.veh^{-1}) [oz TWRP.mile^{-1}.veh^{-1}]
L1 AR-ACFC	SR 101 Loop	E Thomas Rd	1	N/A*
L1 AR-ACFC	SR 101 Loop	E Thomas Rd	2	N/A*
L2 AR-ACFC	SR 101 Loop	E Sweetwater Ave	1	N/A*
L2 AR-ACFC	SR 101 Loop	E Sweetwater Ave	2	N/A*
L3 AR-ACFC	US 60	S Longmore	1	4.47 x 10^{-02} [2.54 x 10^{-06}]
L3 AR-ACFC	US 60	S Longmore	2	3.42 x 10^{-02} [1.94 x 10^{-06}]
L4 AR-ACFC	US 60	S Extension Rd	1	2.80 x 10^{-02} [1.59 x 10^{-06}]
L4 AR-ACFC	US 60	S Extension Rd	2	5.03 x 10^{-02} [2.86 x 10^{-06}]
L5 AR-ACFC	I-17	W Rose Garden Ln	1	4.35 x 10^{-02} [2.47 x 10^{-06}]
L5 AR-ACFC	I-17	W Rose Garden Ln	2	2.11 x 10^{-02} [1.20 x 10^{-06}]
L6 AR-ACFC	I-17	W Utopia Rd	1	2.24 x 10^{-01} [1.27 x 10^{-05}]
L6 AR-ACFC	I-17	W Utopia Rd	2	1.62 x 10^{-01} [9.17 x 10^{-06}]
L1 DG	SR 101 Loop	N 15th Ave	1	4.23 x 10^{-02} [2.40 x 10^{-06}]
L1 DG	SR 101 Loop	N 15th Ave	2	5.65 x 10^{-02} [3.21 x 10^{-06}]
L2 DG	SR 101 Loop	N 64th St	1	2.05 x 10^{-02} [1.16 x 10^{-06}]
L2 DG	SR 101 Loop	N 64th St	2	2.11 x 10^{-02} [1.20 x 10^{-06}]
L3 DG	SR 101 Loop	S McClintock Dr	1	1.18 x 10^{-01} [6.70 x 10^{-06}]
L3 DG	SR 101 Loop	S McClintock Dr	2	1.80 x 10^{-01} [1.02 x 10^{-05}]
L4 DG	SR 101 Loop	W Galveston St	1	N/A*
L4 DG	SR 101 Loop	W Galveston St	2	4.10 x 10^{-02} [2.33 x 10^{-06}]
L5 DG	SR 101 Loop	E Victory Dr	1	1.30 x 10^{-01} [7.41 x 10^{-06}]
L5 DG	SR 101 Loop	E Victory Dr	2	1.99 x 10^{-01} [1.13 x 10^{-05}]

Site ID	Route	Overpass	Sample #	TW EFs (mg TWRP.km^{-1}.veh^{-1}) [oz TWRP.mile^{-1}.veh^{-1}]
L6 DG	SR 101 Loop	W Canal Path	1	3.73 x 10^{-02} [2.12 x 10^{-06}]
L6 DG	SR 101 Loop	W Canal Path	2	4.91 x 10^{-02} [2.79 x 10^{-06}]
L1.1W AR-ACFC	SR 101 Loop	E Thomas Rd	1	2.55 x 10^{-02} [1.45 x 10^{-06}]
L1.2W AR-ACFC	SR 101 Loop	E Thomas Rd	1	2.98 x 10^{-02} [1.69 x 10^{-06}]
L2W AR-ACFC	SR 101 Loop	E Sweetwater Ave	1	9.94 x 10^{-03} [5.64 x 10^{-07}]
L1W DG	SR 101 Loop	N 15th Ave	1	2.61 x 10^{-02} [1.48 x 10^{-06}]
L2W DG	SR 101 Loop	N 64th St	1	5.59 x 10^{-03} [3.17 x 10^{-07}]
L4W DG	SR 101 Loop	W Galveston St	1	5.59 x 10^{-03} [3.17 x 10^{-07}]

*Sites where either tire markers were not detected or the concentration was below the method's detection limit.

Comparison Between DG and AR-ACFC TW Emissions

When comparing EFs between DG and AR-ACFC surfaces, there do not appear to be any obvious differences. This is demonstrated in Figure 24 where both surface types follow a similar EF distribution. The average EF for AR-ACFC surfaces was 0.0609 ± 0.0671 mg TWRP.km^{-1}.veh^{-1} [3.457 x10^{-6} ± 3.810 x10^{-6} oz TWRP.mile^{-1}.veh^{-1}] and the average EF for DG surfaces was 0.0665 ± 0.06338 mg TWRP.km^{-1}.veh^{-1} [3.774 x10^{-6} ± 3.598 x10^{-6} oz TWRP.mile^{-1}.veh^{-1}]; both surfaces are within a standard deviation of each other.

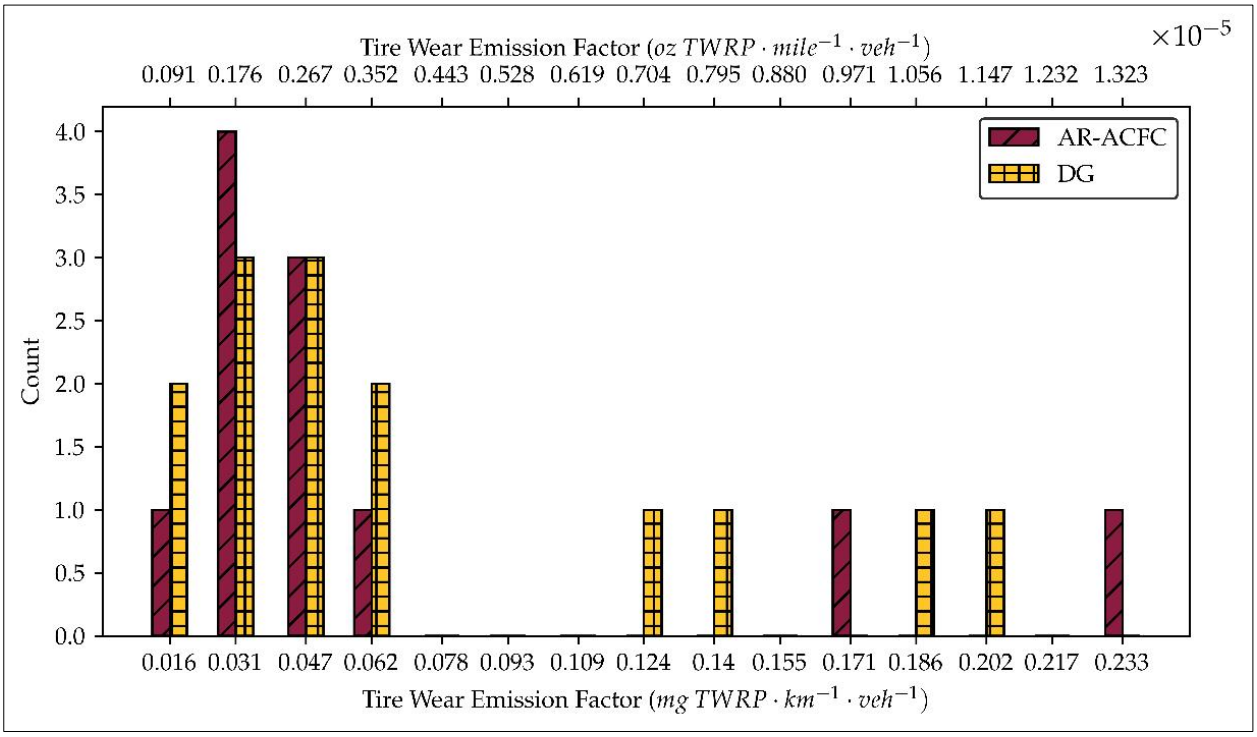

Figure 24. Histogram of TW EFs for AR-ACFC Surfaces Versus DG Surfaces

The research team repeated sampling at five of the sites (repeated twice at one site) during the winter to determine whether environmental factors influence the TW EFs. On average, the ambient temperature on winter sampling days was 29.1° C [84.4° F] cooler than the summer samples, the surface temperature was 37.8° C [100° F] cooler than the summer samples, and the RH was 18.8 percent higher than the summer samples. For all but one of the winter samples, tire markers were not detected. Therefore, the method detection limit of 2PB was used to calculate the potential maximum TW EFs at those sites.

Shown in Figure 25, it is apparent that winter TW EFs are much lower than the summer samples. Additionally, the winter gravimetric PM_{10} was about 29 percent lower than the summer PM_{10}. However, when looking at more short-term environmental changes, such as those between consecutive summer samples (higher temperatures and lower RH for the second sample), no significant differences in EFs were observed.

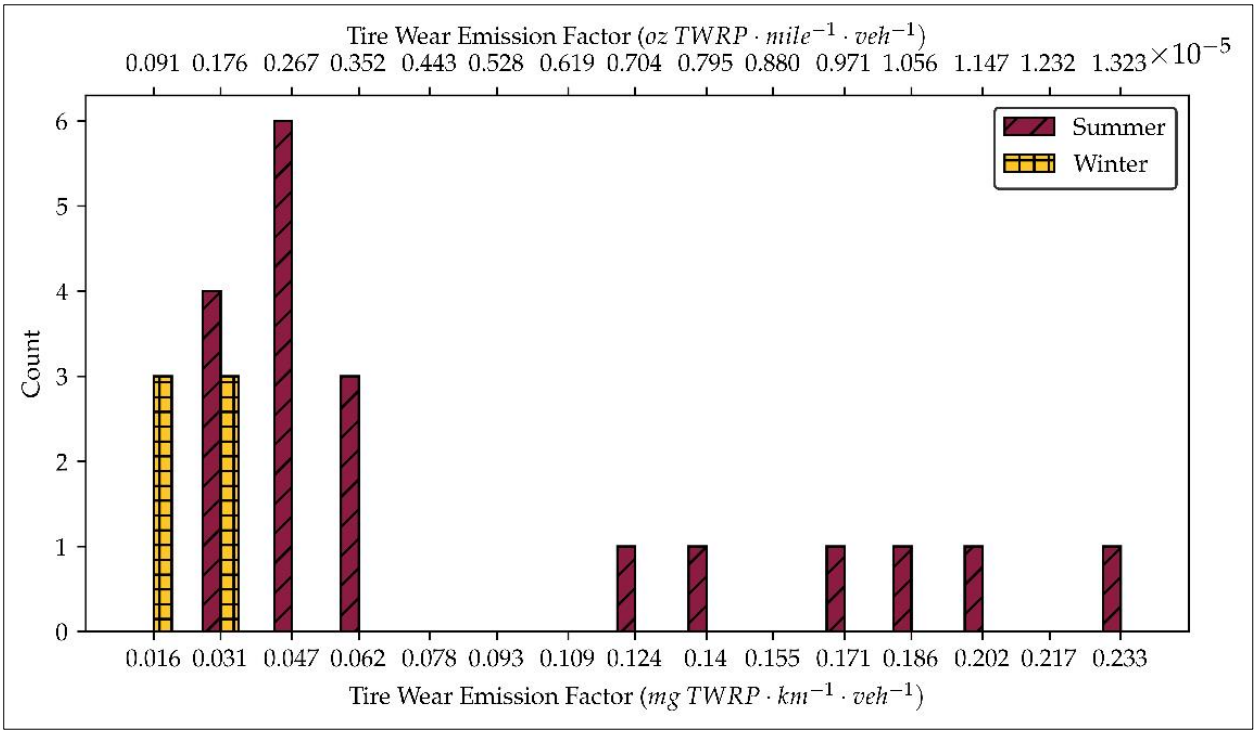

Figure 25. Histogram of TW EFs for Winter Samples Versus Summer Samples

MOVES Simulated EF

After running the MOVES simulations, the output was normalized to obtain PM^{10} and $PM^{2.5}$ TW EFs for each location. The EFs for the summer sampling are shown in Figure 26, while those for winter sampling are shown in Figure 27. The calculated EFs for all sites were similar and with an average of 4.3 mg $TWRP.km^{-1}.veh^{-1}$ (2.44 x 10^{-06} oz $TWRP.mile^{-1}.veh^{-1}$) across both sampling campaigns. This is expected, as the vehicle speed is the major variable that affects TW emissions in MOVES. Vehicle speed on a highway

was assumed to be constant in all simulations. Additionally, the traffic composition did not include any significant HDVs; therefore, it did not have any significant effect on the outcome of the simulations. The slight variation between the sites is minimal and within the expected range of error due to the relatively low precision in MOVES project-level outputs. However, this variation follows the same pattern as the difference in traffic between the sites.

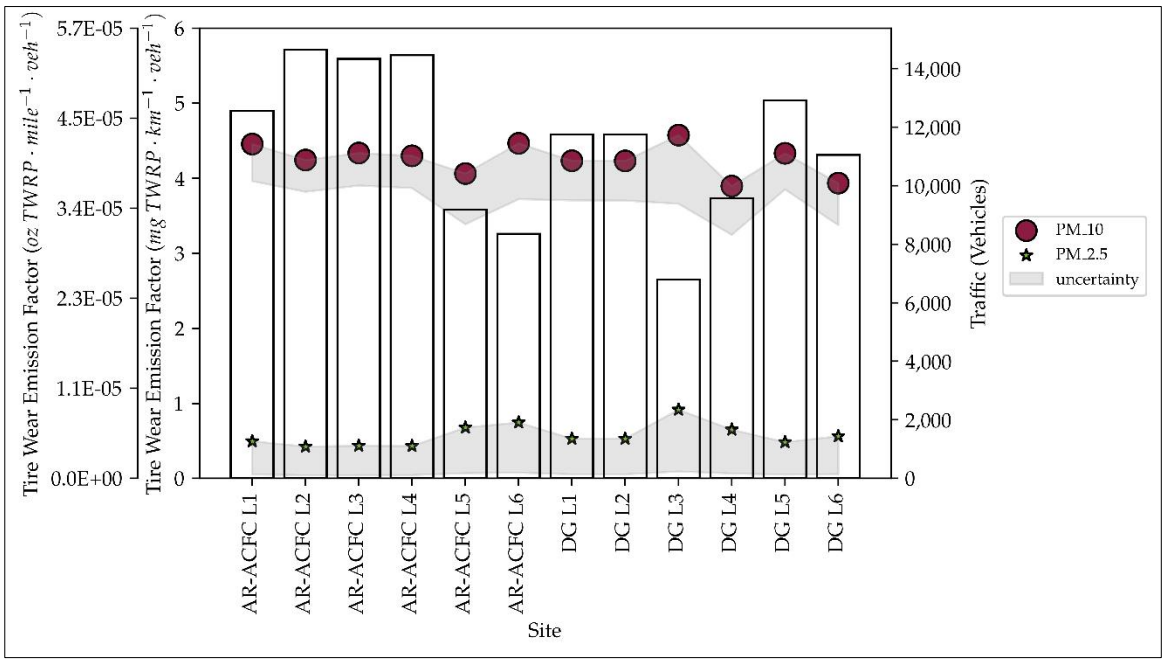

Figure 26. MOVES Simulated TW EFs for the Summer Sampling Sites

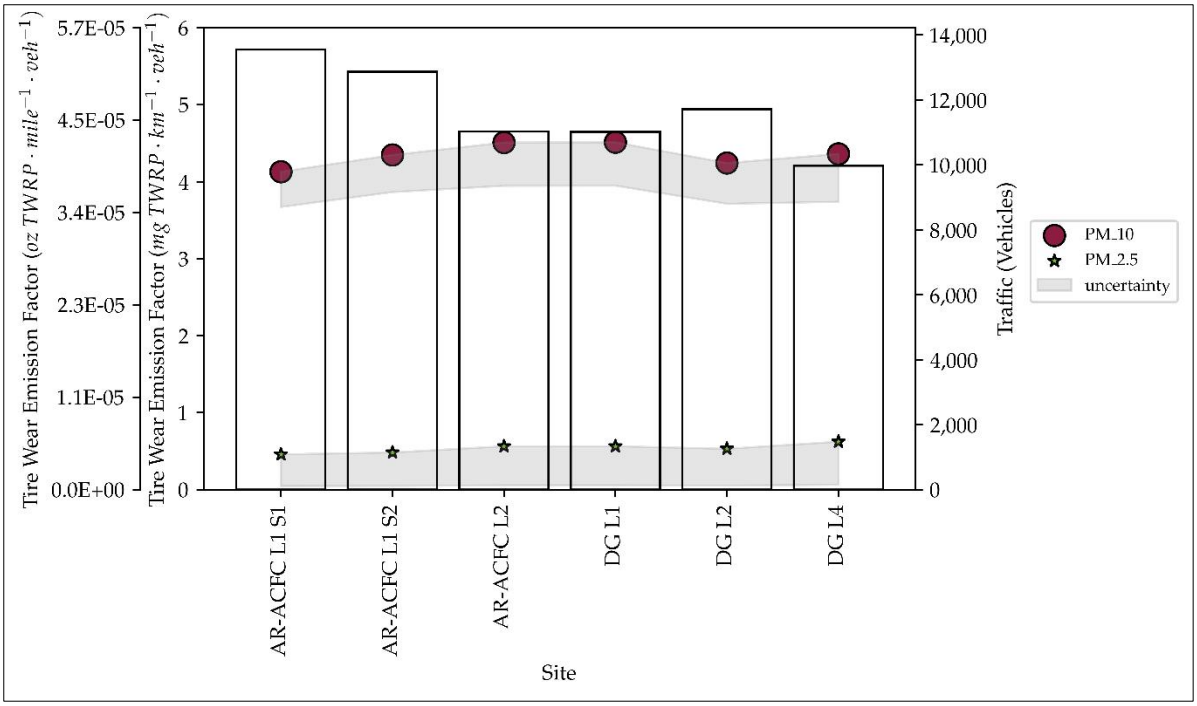

Figure 27. MOVES Simulated TW EFs for the Winter Sampling Sites

The model simulations were not sensitive to the surface type, nor did the simulated EFs follow any particular trend when comparing summer and winter simulations because they were only affected by traffic, as shown in Figure 28.

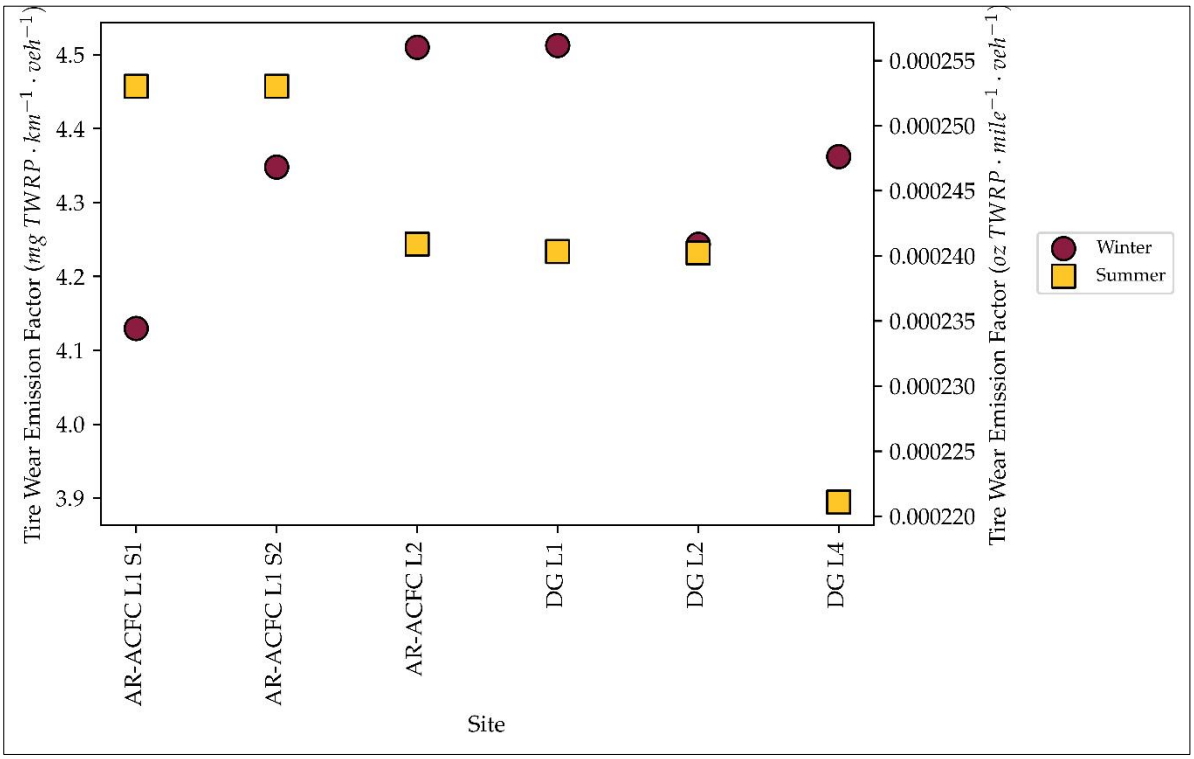

Figure 28. Difference in Simulated EF for the Summer and Winter Sampling Campaigns

The simulated EFs were drastically higher than those measured in the field and were more in line with the higher range of values reported in the literature. Figure 29 presents the ratio of the simulated TW EFs to those calculated from field measurements. The mismatch between the field measurements and predictions can be associated with several factors related to the challenges of sampling operation, identification of markers, unaccounted factors (such as roadway sweeping prior to sampling), and representativeness of the models.

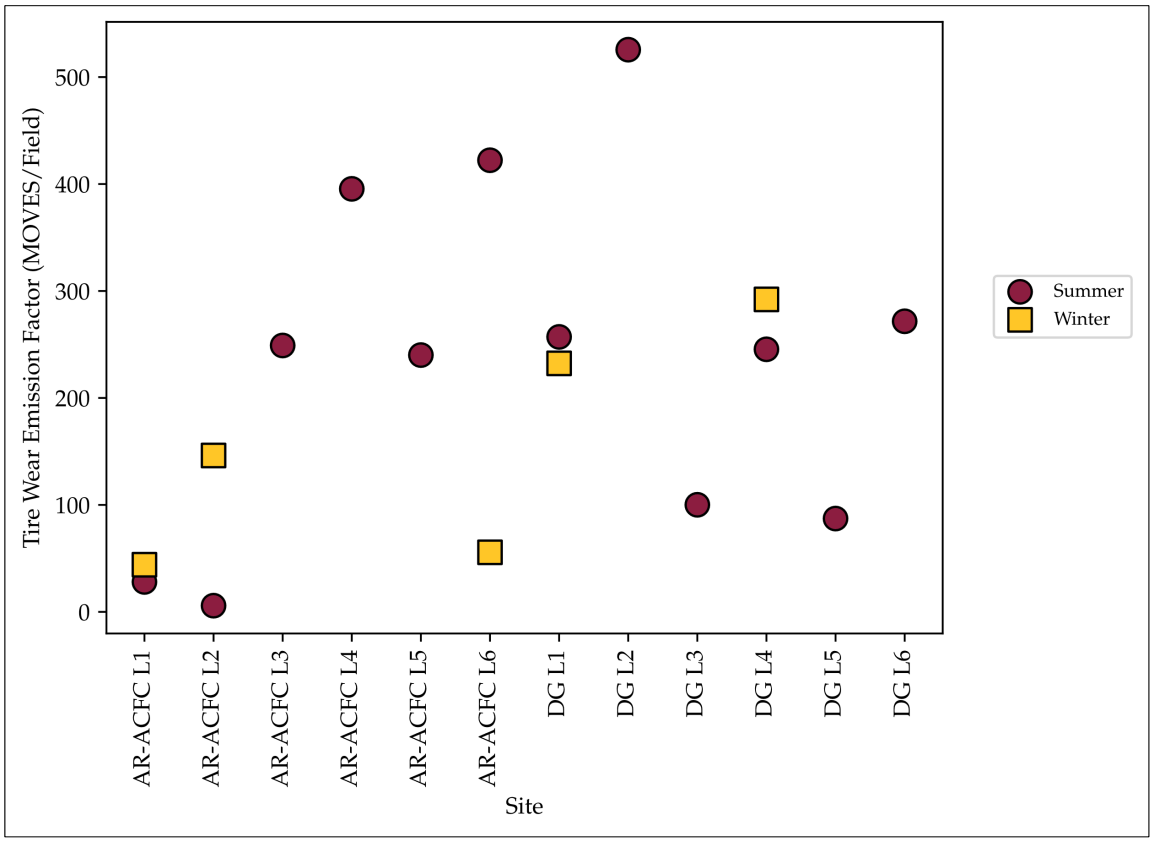

Figure 29. Ratio Between Simulated and Measured TW Emissions

Methods

Overview

The sampling for this study took place on an overpass above a target highway. Sampling equipment included two aerosol samplers that contained a quartz-fiber filter and a cellulose filter, one weather station, and a generator. To correct for atmospheric mixing, the sampling protocol also required positioning and burning flares on the highway under the overpass to account for air dilution and transport from the road to the sampler. For each sampling site, 11 flares were positioned on the highway every 50 feet. The flares were replaced every 30 minutes during the total two-hour sampling period. A total of 44 flares were used for each site. The airborne particles collected by the two aerosol samplers were then extracted from the filter in the laboratory and analyzed using gas chromatography–mass spectrometry. The overall methodology is shown in Figure 30.

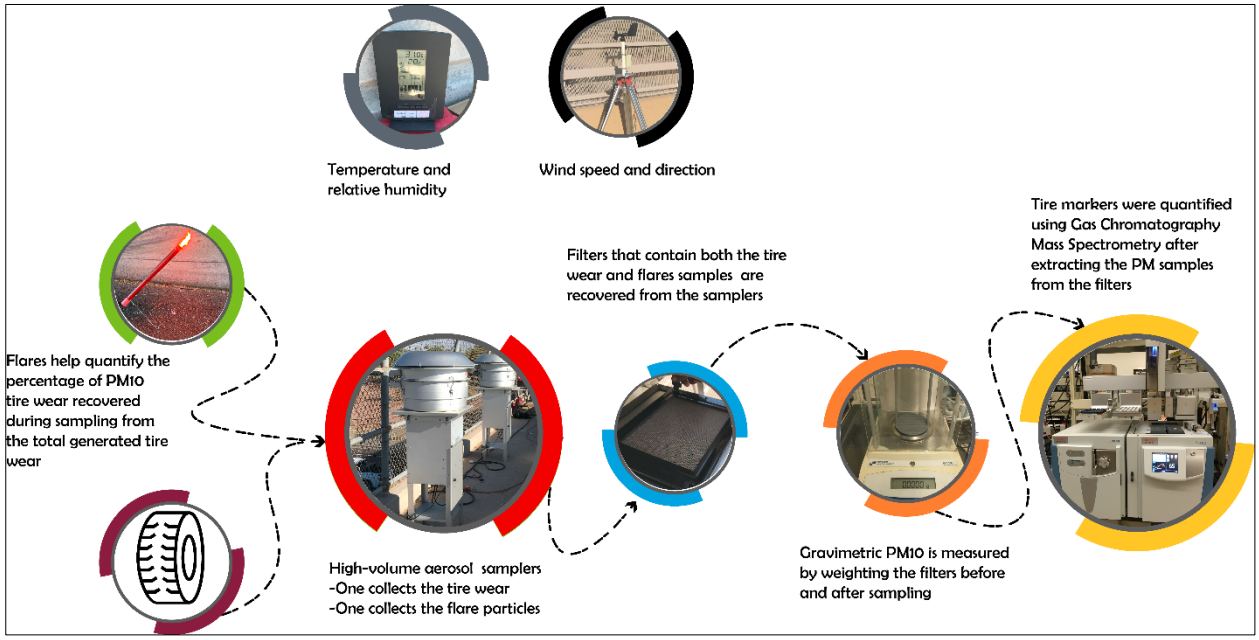

Figure 30. TW Emissions Measurement Methodology

Field Sampling

Site Selection

The site-selection methodology included factors that could affect TW based on the findings from the literature review presented in Appendix A. These factors included traffic volume and composition, pavement condition, and the feasibility of a safe and robust sampling operation.

Traffic and Environmental Conditions

Hourly traffic was counted at 10-minute intervals by traffic counters that could measure traffic volume and traffic composition in both directions, as shown in Figure 31 and Figure 32. FHWA vehicle classifications and the distribution of traffic among lanes were also monitored throughout sampling. A commercial electric infrared thermometer was used to measure the pavement surface temperatures periodically throughout sampling. Wind speed values were measured using a RainWise™, Inc., WindLog© Wind Data Logger.

Figure 31. Setting Up Traffic Control at the Victory Drive Site and Traffic Counters Installed on a Pole

Figure 32. Setting Up Traffic Control at the Victory Drive Site and Traffic Counters Installed on a Pole

TW PM_{10} Sampling

Figure 33 demonstrates the sampling setup at a typical site. Sampling equipment was in the middle of the overpass and flares, as shown in Figure 34, were deployed in the HOV lane, which was closed with traffic control devices. Figure 35 and Figure 36 also show an overview of the sampling operation at the overpass and highway from Galveston Road and Rose Garden sites. The sampling equipment included two high-volume PM_{10} samplers, one to collect the TW on a quartz-fiber filter and the other to collect the flare particles on a cellulose filter. Other equipment, such as a weather station to measure ambient temperature and RH and a wind speed and direction sensor, were also used. Two one-hour samples were collected at 12 sites in the summer, with the original goal being to capture different traffic conditions from just after rush hour (08:30–09:30 a.m.) compared to a bit later (10:00–11:00 a.m.). However, after initial traffic results were analyzed, there was little difference in traffic volumes between these times, so a single two-hour sampling period was used during the winter to maximize the amount of material collected onto the filters.

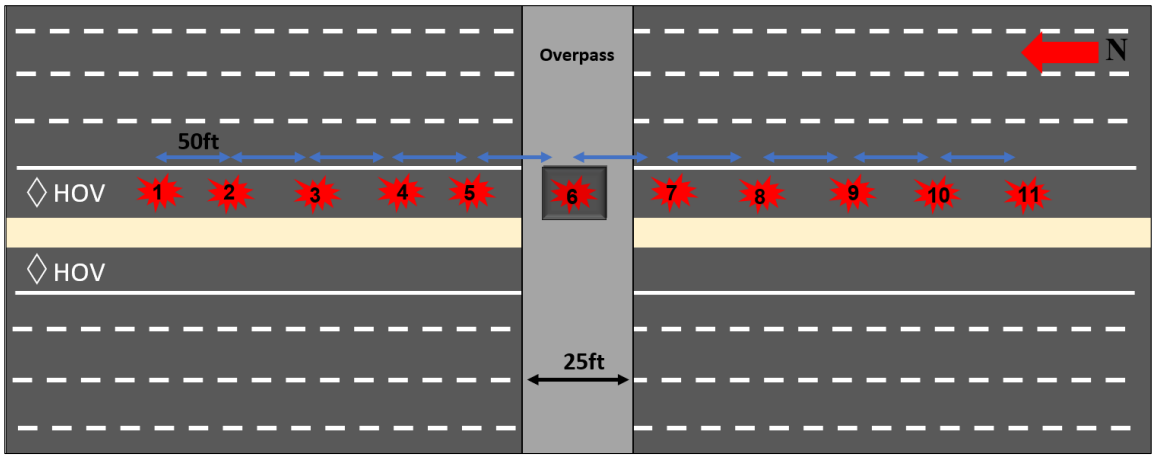

Figure 33. Schematic of the Sampling Setup—
Four Flares Were Placed at Each Red Marker, Placed 50 ft Apart

Figure 34. Burning Flares in the HOV Lane During Sampling

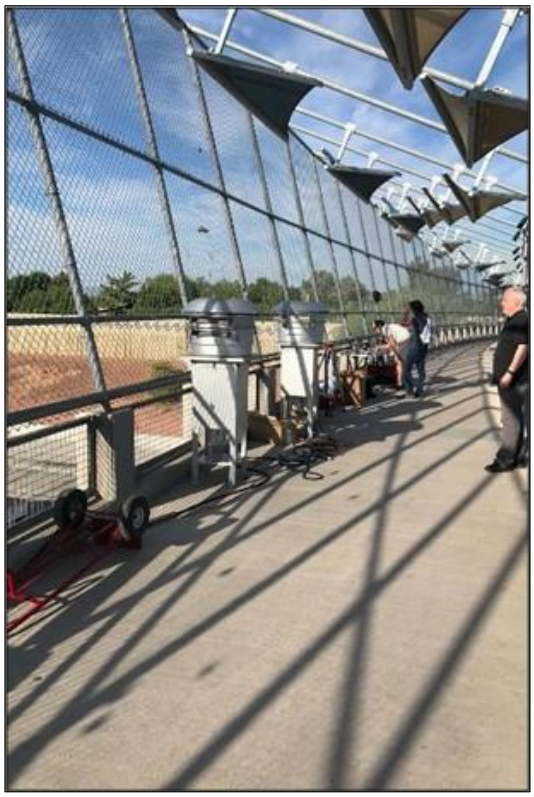

Figure 35. Sampling Operation at Galveston Rd. Pedestrian Overpass

Figure 36. Overview of Rose Garden Site

Used-tire Sample Collection and Processing

Sixteen used-tire samples were obtained from CRM of America™, LLC, in Queen Creek, Arizona, with a 50:50 split between LDV and HDV (Figure 37 and Table 8). These samples were ground with a grinding power tool and the resulting PM_{10} was collected on a pre-weighed and pre-baked 37-mm quartz filter with a low-volume air sampler using a PM_{10} Cyclone© (URG Corporation™, Chapel Hill, NC) as the size-cut.

Figure 37. Tire Source and Manufacturer Collected from CRM of America, LLC

Table 8. Tire Source and Manufacturer Collected from CRM of America, LLC

Sample #	Brand (all TM)	Make (all ©)	Type
1	Michelin	Defender XT	LDV
2	Michelin	Latitude Tour HP	LDV
3	Goodyear	Eagle Touring	LDV
4	Goodyear	Reliant	LDV
5	Yokohama	YK740 GTX	LDV
6	Yokohama	YK-HTX	LDV
7	Nitto	Ridgegrapler	LDV (hybrid terrain)
8	Nitto	Ridgegrapler	LDV (hybrid terrain)
10	Bridgestone	ECOPIA H-DRIVE 002	HDV
11	Bridgestone	L320	HDV
12	Goodyear	G314 LHT	HDV
13	Goodyear	Endurance LHD	HDV
14	Hankook	E3 Max TL 21	HDV
15	Hankook	E3 Max TL 21	HDV
16	Toyo	M122	HDV
17	Toyo	M154	HDV

Laboratory Characterization

Tire Markers Identification

Prior to extraction, the highway filters were cut into eighths, half of which were returned to their aluminum foil pouch and placed in the freezer and the other half extracted as the sample analysis does not require the full filter and also to act as a back-up in case the original analysis produces anomalous results. The resuspended tire samples were fully extracted. For each extraction, 50 µL [0.00169 fl oz] of an internal standard, used for quality-assurance purposes, was dropped onto the filter sections and allowed to dry. Samples were extracted three times with 30–40 mL [1.01–1.35 fl oz] of dichloromethane under sonication for 15 minutes. The combined extracts were evaporated under Nitrogen gas (N_2) to ~5 mL [0.169 fl oz]. The extract solution was filtered using a pre-baked quartz-fiber filter, evaporated further down to 100 µL [0.00338 fl oz], and transferred to a vial with a glass insert and kept in the freezer until analysis.

Chemical tire markers were quantified in the extracted PM samples using gas chromatography–mass spectrometry (GC–MS), as shown in Figure 38. These markers were identified and quantified using authentic standards of 2PB, N-cyclohexyl-2-benzothiazolamine, benzothiazole, and 2-hydroxybenzothiazole. The 2PB method detection limit was determined by seven consecutive GC–MS runs of a low-concentration 2PB standard.

Figure 38. GC–MS Device

Gravimetric PM_{10} Concentrations

Gravimetric PM_{10} concentrations from each sample were determined by weighing the filters in triplicate before and after sampling. The mass difference for each sample was then divided by the volume of air sampled (calculated from the sampler flow rate and sample time) to obtain PM_{10} concentrations.

Sr From Flares

Sr mass concentrations of highway samples were determined using inductively coupled plasma mass spectrometry (ICP–MS) after a microwave-assisted acid digestion on the sampled cellulose filters.

Emission Rate Calculation and Verification

TW EFs were calculated using Equation 1. The value of 0.0947 miles arises from the length of the flare-line source used at every sampling site. This represents the effective distance of road that was sampled. The TW emission rate was calculated using Equation 2. The weighted average 2PB composition was discussed in the *Tire Marker Findings* section. The theoretical Sr mass emitted was calculated by multiplying the number of flares lit during the sample by the average Sr mass emitted by flares during testing (501,620 nanograms).

$$EF\left(\frac{mg\ [ounce]}{miles \times vehicles}\right) = \frac{\left[Tire\ Wear\ Emission\ Rate\left(\frac{mg\ [ounce]}{minute}\right) \times Sample\ Time\ (minutes)\right]}{(0.0947\ miles \times \#vehicles)} \quad \text{Eq. 1}$$

$$Tire\ Wear\ Emission\ Rate\ \left(\frac{mg\ [ounce]}{minute}\right) = \frac{\frac{2PB\ Mass\ on\ Filter\ (mg\ [ounce])}{\left(\frac{Weighted\ Average\ 2PB\ Tire\ Composition\ \%}{100}\right)}}{\frac{\left(\frac{Sr\ on\ Whole\ Filter\ (ng\ [ounce])}{Theoretical\ Sr\ Mass\ Emitted\ (ng\ [ounce])}\right)}{Time\ Sampled\ (minutes)}} \quad \text{Eq. 2}$$

Emission Modeling

MOVES is an emission-modeling software program developed by the EPA to quantify air-pollution emissions that are emitted from motor vehicles. MOVES can be used to model and estimate the emissions of carbon monoxide, nitrogen oxides, volatile organic compounds, and PM along with other pollutants coming from road vehicles like cars, trucks, and motorcycles, and other non-road vehicles like tractors and agricultural equipment. MOVES has been heavily used by a wide range of transportation stakeholders, including agencies, researchers, consultants, and policymakers, to make informed decisions that support emission-reduction strategies on local, state, and regional levels. MOVES' structure is illustrated in Figure 39.

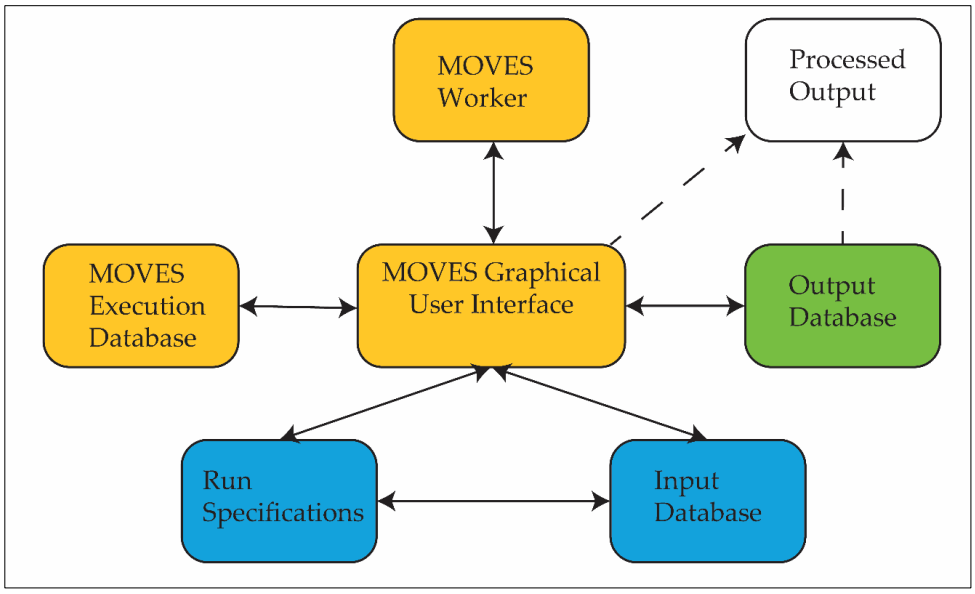

Figure 39. MOVES Structure (Adapted from Kang (2013))

MOVES utilizes a simple TW model to estimate TW emissions. The procedure is outlined in Figure 40. TW is calculated based on a simple regression model that incorporates vehicle speed as a single variable. After calculating the TW, the PM_{10} portion of the particulate matter is assumed to be 8 percent of the total TW based on the findings of earlier studies (Luhana et al. 2004, Kupiainen et al. 2005). Approximately 15 percent of the total PM_{10} is assumed to have a diameter of less than 2.5 µm. Vehicle classification is accounted for by the number of tires each vehicle has. Vehicle speed and traffic counts are the primary factors that affect TW in MOVES simulations, as shown in Figure 41.

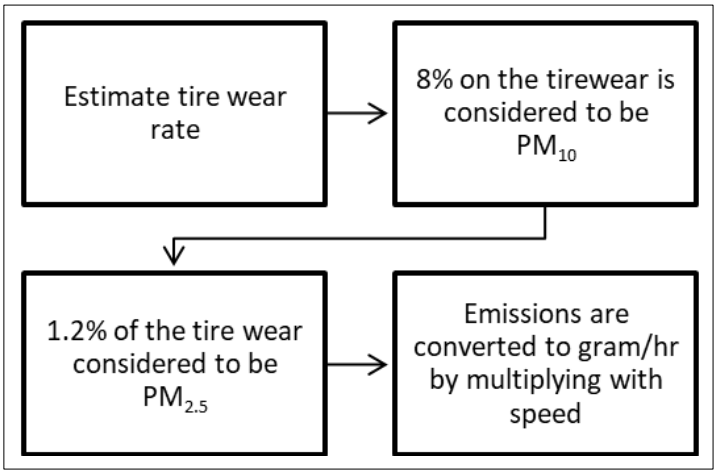

Figure 40. EPA MOVES TW Emissions Model

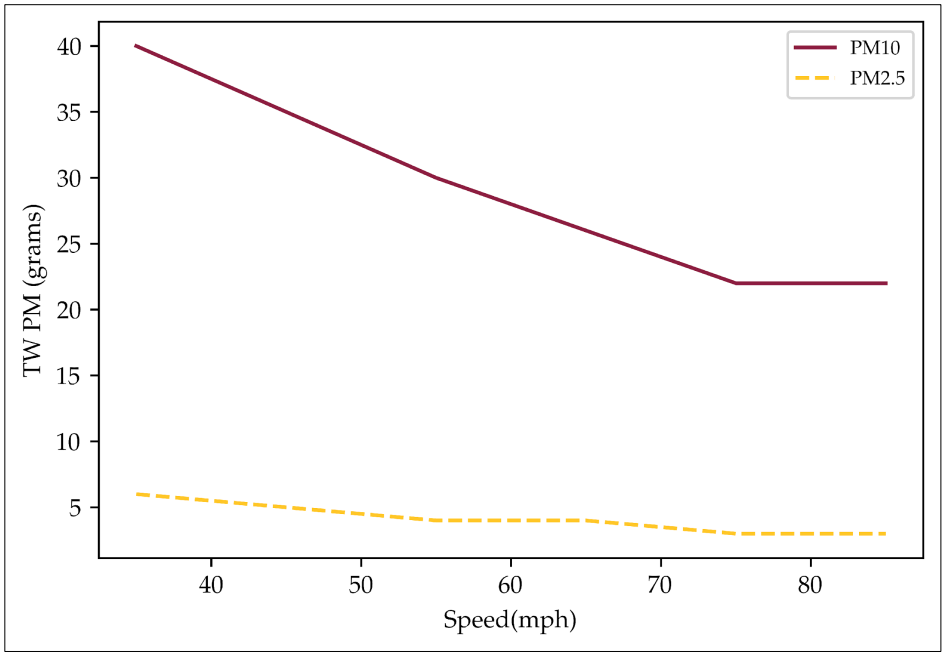

Figure 41. MOVES Simulation for the Generated Amount of TW Emissions with Variable Speed

Data Collection and Preparation

The research team conducted project-scale analysis to obtain TW EFs for all sampled sites in order to compare the simulated TW emissions with the emissions derived from the field measurements.

MOVES requires variable inputs to simulate TW emissions. Some inputs are required to calculate total emissions, while others are necessary to calculate exhaust PM_{10} emissions, which are a prerequisite for running any TW emissions simulations. Some of these inputs and the sources of the used data are introduced in Table 9.

Table 9. MOVES Input Data for Project-level Analysis

Variable	Input	Source
Time Span	Month and year of Sampling	Field Sampling
Geographic Bounds	Maricopa County, AZ	Field Sampling
Road Type	Urban Unrestricted Access	Field Sampling
Link Length	Distance between flares	Field Sampling
Volume	Total counted traffic	Field Sampling
Link Average Speed	Speed on the Highway (65 mph)	Assumption
Link Average Grade	Highway Slope (0)	Assumption
Temperature and Humidity	Environmental conditions Highway	Field Sampling
Relative Humidity	Environmental conditions Highway	Field Sampling
Age Distribution of Vehicles	Percentage of age of vehicle. A sample is provided in Figure 42.	Provided by Maricopa Association of Governments (MAG)

Variable	Input	Source
Inspection/Maintenance Values	Inspection and Maintenance	Provided by MAG
Fuel	Fuel composition in AZ	Provided by MAG
Source Type	Vehicle Classification	Field Sampling

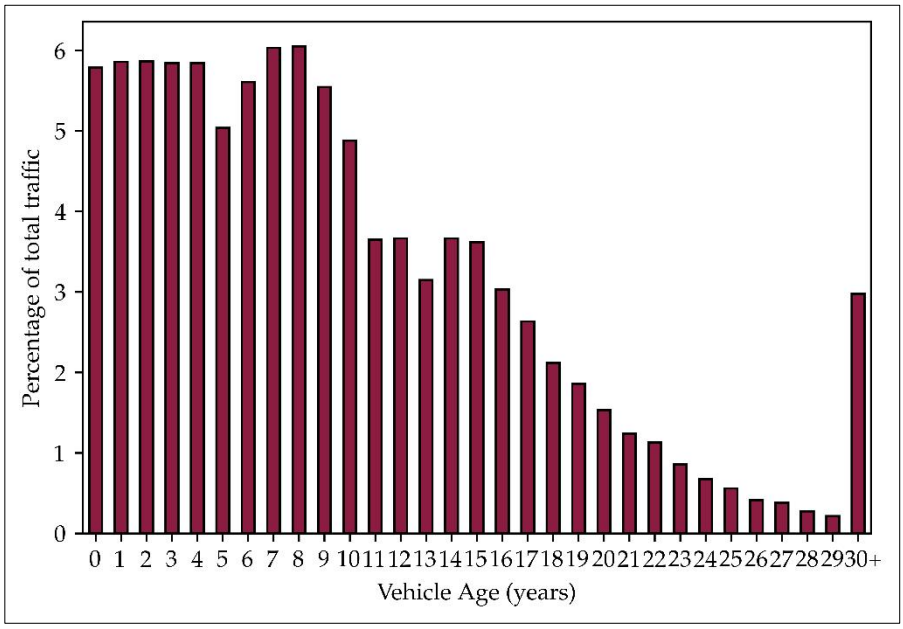

Figure 42. Vehicle Age Distribution

MOVES uses a slightly different vehicle classification system from that of FHWA. However, the vehicle classes were interrelated for the purposes of this report, as shown in Table 10.

Table 10. MOVES Classes Counterparts in FHWA Classification

MOVES Class	Vehicle Type	FHWA Assumed Class	MOVES Class	Vehicle Type	FHWA Assumed Class
11	Motorcycle	1	51	Refuse Truck	—
21	Passenger Car	2	52	Single-unit Short-haul Truck	—
31	Passenger Truck	3	53	Single-unit Long-haul Truck	6–10
32	Light Commercial Truck	5	54	Motor Home	—
41	Other Buses	4	61	Combination Short-haul Truck	—
42	Transit Bus	—	62	Combination Long-haul Truck	11–13
43	School Bus	—	—	—	—

Acknowledgments

This project was conducted as a cooperation between Arizona Department of Transportation; Maricopa Association of Governments; Arizona State University; and Kimley-Horn. The research team acknowledges the technical support received from ADOT's senior research project manager Bill Stone, MAG's air-quality modeling program manager Taejoo Shin; the project's Technical Advisory Committee; ADOT's Tempe Maintenance Yard and ADOT's Happy Valley Maintenance Yard.

The authors would like to acknowledge the assistance provided by ASU's researchers and students who aided in the field sampling conducted in this study: Jesse Molar, Zhaobo Zhang, Kanchana Chandrakanthan, Thuong Cao, Gabrielle Cano, Parker Abel, Aidan McClure, Amelia Stout, Ramadan Salim, Ashraf Alrajhi, Naagaviswanath Vedula, and Masih Beheshti.

References

Aatmeeyata, D S Kaul, and Mukesh Sharma 2009. “Traffic Generated Non-Exhaust Particulate Emissions from Concrete Pavement: A Mass and Particle Size Study for Two-Wheelers and Small Cars.” Atmospheric Environment, 43 (35), 5691–5697.

Abu-Allaban, M., Gillies, J.A., Gertler, A.W., Clayton, R., and Proffitt, D., 2003. “Tailpipe, Resuspended Road Dust, and Brake-Wear Emission factors from on-road vehicles.” Atmospheric Environment, 37 (37), 5283–5293.

Alexandrova, Olga, Kamil E Kaloush, and Jonathan O Allen. 2007. “Impact of Asphalt Rubber Friction Course Overlays on Tire Wear Emissions and Air Quality Models for Phoenix, Arizona,” Airshed. Transportation Research Record: Journal of the Transportation Research Board, 2011 (1), 98–106.

Allen, Jonathan O., Olga Alexandrova, and Kamil E. Kaloush. 2006. “Tire wear emissions for asphalt rubber and Portland cement concrete pavement surfaces.”

Alves, Célia Anjos, A M P Vicente, Ana Isabel Calvo, Darrel Baumgardner, Fulvio Amato, Xavier Querol, Casimiro Pio, and Mats Gustafsson. 2020. “Physical and chemical properties of non-exhaust particles generated from wear between pavements and tyres.” Atmospheric environment (1994), 224, 117252.

Amann, Markus, Janusz Cofala, Chris Heyes, Zbigniew Klimont, Reinhard Mechler, Maximilian Posch, and Wolfgang Schöpp. 2004. “The Regional Air Pollution Information and Simulation (RAINS) Model.” Interim Report, IIASA, Laxenburg, Austria. http://www. iiasa. ac. at/rains/review/review-full. pdf.

Amato, Fulvio, Alexandros, Alexandros Dimitropoulos., Katherine Farrow, Walid Oueslati, and the Organisation for Economic Co-operation and Development (OECD), 2020. “Non-exhaust Particulate Emissions from Road Transport: An Ignored Environmental Policy Challenge.” Organisation for Economic Co-operation and Development.

Amato, Fulvio, Olivier Favez, Marco Pandolfi, Andrés Alastuey, Xavier Querol, Sophie Moukhtar, Benjamin Bruge, Stephane Verlhac, Jose Antonio Garcia Orza, Nicolas Bonnaire, Tiphaine Le Priol, Jean-Eudes Petit, and Jean Sciare, 2016. “Traffic induced particle resuspension in Paris: Emission factors and source contributions.” Atmospheric Environment, 129, 114–124.

Avagyan, Rozanna, Ioannis Sadiktsis, Gunnar Thorsén, Conny Östman, and Roger Westerholm 2013. “Determination of benzothiazole and benzotriazole derivates in tire and clothing textile samples by high performance liquid chromatography–electrospray ionization tandem mass spectrometry.” Journal of Chromatography A, 1307, 119–125.

Baensch-Baltruschat, Beate, Birgit Kocher, Friederike Stock, and Georg Reifferscheid. 2020. “Tyre and road wear particles (TRWP) - A review of generation, properties, emissions, human health risk, ecotoxicity, and fate in the environment.” Science of The Total Environment, 733, 137823.

Barbin, W.W. and Rodgers, M.B., 1994. “The Science of Rubber Compounding.” Science and Technology of Rubber. Elsevier, 419–469.

Barlow, Tim. 2014. “Briefing Paper on Non-exhaust Particulate Emissions from Road Transport.” Transport Research Laboratory, Wokingham, UK.

Barnes, K.A., Castle, L., Damant, A.P., Read, W.A., and Speck, D.R., 2003. “Development and application of an LC–MS method to determine possible migration of mercaptobenzothiazole, benzothiazole and related vulcanization residues from rubber used in contact with food and drink.” Food Additives & Contaminants, 20 (2), 196–205.

Beddows, David C.S., and Roy M. Harrison. 2021. “PM_{10} and $PM_{2.5}$ emission factors for non-exhaust particles from road vehicles: Dependence upon vehicle mass and implications for battery electric vehicles. Atmospheric Environment, 244, 117886.

Cadle, S.H. and R.L. Williams. 1978. “Gas and Particle Emissions from Automobile Tires in Laboratory and Field Studies.” Journal of the Air Pollution Control Association, 28 (5), 502–507.

Callender, Edward, and Karen C. Rice. 2000. “The Urban Environmental Gradient: Anthropogenic Influences on the Spatial and Temporal Distributions of Lead and Zinc in Sediments.” Environmental Science & Technology, 34 (2), 232–238.

Councell, Terry B., Kea U. Duckenfield, Edward R. Landa, and Edward Callender. 2004. “Tire-Wear Particles as a Source of Zinc to the Environment.” Environmental Science & Technology, 38 (15), 4206–4214.

Denier van der Gon, Hugo A.C., Miriam E. Gerlofs-Nijland, Robert Gehrig, Mats Gustafsson, Nicole Janssen, Roy M. Harrison, Jan Hulskotte, Jan Hulskotte, Christer Johansson, Magdalena Jozwicka, Menno Keuken, Klaas Krijgsheld, Leonidas Ntziachristos, Michael Riediker & Flemming R. Cassee. 2013. “The Policy Relevance of Wear Emissions from Road Transport, Now and in the Future—An International Workshop Report and Consensus Statement.” Journal of the Air & Waste Management Association, 63 (2), 136–149.

Fauser, Patrik. 1999. “Particulate air pollution with emphasis on traffic generated aerosols.” Roskilde: Risø National Laboratory.

Fiala, Matthew, and Hyun-Min Hwang. 2021. “Influence of Highway Pavement on Metals in Road Dust: A Case Study in Houston, Texas.” Water, Air, & Soil Pollution, 232 (5), 185.

Franklin, Emily B., Michael R. Alves, Alexia N. Moore, Delaney B. Kilgour, Gordon A. Novak, Kathryn Mayer, Jonathan S. Sauer, et al. 2021. “Atmospheric Benzothiazoles in a Coastal Marine Environment.” Environmental Science & Technology, 55 (23), 15705–15714.

Gehrig, R., Hüglin, C., and Hofer, P., 2001. “Contributions of Road Traffic to Ambient PM_{10} and $PM_{2.5}$ concentrations.” In: 1st Swiss Transport Research Conference, Monet Verita/Ascona. 1–3.

Gehrig, R., K. Zeyer, N. Bukowiecki, P. Lienemann, L.D. Poulikakos, M. Furger, and B. Buchmann. 2010. “Mobile load simulators – A tool to distinguish between the emissions due to abrasion and resuspension of PM_{10} from road surfaces.” Atmospheric Environment, 44 (38), 4937–4943.

Goodarzi, Avesta, and Amir Khajepour. 2017. “Vehicle suspension system technology and design.”

Grigoratos, Theodoros, Mats Gustafsson, Olle Eriksson, and Giorgio Mar. 2018. “Experimental investigation of tread wear and particle emission from tyres with different treadwear marking.” Atmospheric Environment, 182, 200–212.

Grigoratos, Theodoros, and Giorgio Martini. 2014. “Non-exhaust traffic related emissions—Brake and tyre wear PM literature review.” Italy: European Commission, Institute for Energy and Transport.

Gustafsson, Mats, Christer Johansson, Sverige, and Trafikverket.2012. “Road pavements and PM_{10}. Summary of the results of research funded by the Swedish Transport Administration on how the properties of road pavements influence emissions and the properties of wear particles. Retrieved from Trafikverket website: https://urn.kb.se/resolve?urn=urn:nbn:se:vti:diva-5373

Gustafsson, Mats, Lars Kraft, and Johan Silfwerbrand. 2015. “Wear and Particle Generation of Three Pavement Alternatives, a Reference Concrete, an Experimental Photocatalytic Concrete, and a Standard Asphalt Pavement.”

Harrison, Roy M., James Allan, David Carruthers, Mathew R. Heal, Alastair C. Lewis, Ben Marner, Tim Murrells, and Andrew Williams. 2021. “Non-exhaust vehicle emissions of particulate matter and VOC from road traffic: A review. Atmospheric Environment, 262, 118592.

Hicks, William, Sean Beevers, Anja H Tremper, Gregor Stewart, Max Priestman, Frank J Kelly, Mathias Lanoisellé, Dave Lowry, and David C Green. 2021. “Quantification of Non-Exhaust Particulate Matter Traffic Emissions and the Impact of COVID-19 Lockdown at London Marylebone Road.” Atmosphere.

Johansson, Christer, Michael Norman, and Lars Gidhagen. 2007. “Spatial & temporal variations of PM_{10} and particle number concentrations in urban air.” Environmental Monitoring and Assessment, 127 (1–3), 477–487.

Kang, Seunggu. 2013. “The development of a regional inventory database for the material phase of the pavement life-cycle with updated vehicle emission factors using MOVES.”

Karagulian, Federico, Claudio A. Belis, Carlos Francisco C. Dora, Annette M. Prüss-Ustün, Sophie Bonjour, Heather Adair-Rohani, Markus Amann. 2015. “Contributions to cities’ ambient particulate matter: A systematic review of local source contributions at global level.” Atmospheric Environment, 120, 475–483.

Keuken, Menno, Hugo Denier van der Gon, and Karin van der Valk. 2010. “Non-exhaust emissions of PM and the efficiency of emission reduction by road sweeping and washing in the Netherlands.” Science of The Total Environment, 408 (20), 4591–4599.

Kim, Gibaek, and Seokhwan Lee. 2018. “Characteristics of Tire Wear Particles Generated by a Tire Simulator under Various Driving Conditions.” Environmental Science & Technology, 52 (21), 12153–12161.

Kim, Man Goo, Kazuo Yagawa, Hidenari Inoue, Yong Keun Lee, and Tsuneo Shirai. 1990. “Measurement of tire tread in urban air by pyrolysis-gas chromatography with flame photometric detection.” Atmospheric Environment. Part A. General Topics, 24 (6), 1417–1422.

Klüppel, Manfred. 2014. “Wear and Abrasion of Tires.” In: S. Kobayashi and K. Müllen, eds. Encyclopedia of Polymeric Nanomaterials. Berlin, Heidelberg: Springer Berlin Heidelberg, 1–6.

Knight, Lydia J., Florence N. F. Parker-Jurd, Maya Al-Sid-Cheikh, and Richard C. Thompson. 2020. “Tyre wear particles: an abundant yet widely unreported microplastic?” Environmental Science and Pollution Research, 27 (15), 18345–18354.

Kreider, Marisa L., Julie M. Panko, Britt L. McAtee, Leonard I. Sweet, and Brent L. Finley. 2010. “Physical and chemical characterization of tire-related particles: Comparison of particles generated using different methodologies.” Science of The Total Environment, 408 (3), 652–659.

Kumata, H., Sanada, Y., Takada, H., and Ueno, T., 2000. “Historical Trends of N -Cyclohexyl-2-benzothiazolamine, 2-(4-Morpholinyl)benzothiazole, and Other Anthropogenic Contaminants in the Urban Reservoir Sediment Core.” Environmental Science & Technology, 34 (2), 246–253.

Kumata, Hidetoshi, Hideshige Takada, and Norio Ogura. “Determination of 2-(4-Morpholinyl)benzothiazole in Environmental Samples by a Gas Chromatograph Equipped with a Flame Photometric Detector.” Analytical Chemistry, 68 (11), 1976–1981.

Kumata, Hidetoshi, Junya Yamada, Kouji Masuda, Hideshige Takada, Yukio Sato, Teruaki Sakurai, and Kitao Fujiwara. 2002. “Benzothiazolamines as Tire-Derived Molecular Markers: Sorptive Behavior in Street Runoff and Application to Source Apportioning.” Environmental Science & Technology, 36 (4), 702–708.

Kupiainen, Kaarle J, Heikki Tervahattu, Mika Räisänen, Timo Mäkelä, Minna Aurela, and Risto Hillamo. 2005. “Size and Composition of Airborne Particles from Pavement Wear, Tires, and Traction Sanding.” Environmental Science & Technology, 39 (3), 699–706.

Kwak, Ji-hyun, Hongsuk Kim, Janghee Lee, Seokhwan Lee. 2013. “Characterization of non-exhaust coarse and fine particles from on-road driving and laboratory measurements.” Science of The Total Environment, 458–460, 273–282.

Lawrence, Samantha, Ranjeet Sokhi, Khaiwal Ravindra, Hongjun Mao, Hunter Douglas Prain, Ian D. Bull. 2013. “Source apportionment of traffic emissions of particulate matter using tunnel measurements.” Atmospheric Environment, 77, 548–557.

Lee, Yong-Keun, Man Goo Kim, and Kyu-Ja Whang. 1989. “Simultaneous determination of natural and styrene-butadiene rubber tire tread particles in atmospheric dusts by pyrolysis-gas chromatography.” Journal of Analytical and Applied Pyrolysis, 16 (1), 49–55.

Lee, Youn Suk, Won-Ki Lee, Seong-Gyu Cho, Il Kim, and Chang-Sik Ha. 2007. “Quantitative analysis of unknown compositions in ternary polymer blends: A model study on NR/SBR/BR system.” Journal of Analytical and Applied Pyrolysis, 78 (1), 85–94.

Lowne, R.W., 1970. “The effect of road surface texture on tyre wear.” Wear, 15 (1), 57–70.

Luhana, L., Sokhi, R., Warner, L., Mao, H., Boulter, P., McCrae, I., Wright, J., and Osborn, D., 2004. “Characterisation of exhaust particulate emissions from road vehicles.” FP5 particulates project.

MAG, 2012. “MAG 2012 Five Percent Plan for PM-10 for the Maricopa County Nonattainment Area.”

Oroumiyeh, Farzan, Michael Jerrett, Irish Del Rosario, Jonah Lipsitt, Jonathan Liu, Suzanne E. Paulson, Beate Ritz, James J Schauer, Martin M Shafer, Jiaqi Shen, Scott Weichenthal, Sudipto Banerjee, Yifang Zhu. 2022. "Elemental composition of fine and coarse particles across the greater Los Angeles area: Spatial variation and contributing sources." Environmental Pollution, 292, 118356.

Oroumiyeh, Farzan, and Yifang Zhu. 2021. "Brake and tire particles measured from on-road vehicles: Effects of vehicle mass and braking intensity." Atmospheric Environment: X, 12, 100121.

O'Shea, Michael J., David R. Vann, Wei-Ting Hwang, and Reto Gieré. 2020. "A mineralogical and chemical investigation of road dust in Philadelphia, PA, USA." Environmental Science and Pollution Research, 27 (13), 14883–14902.

Ozaki, Hirokazu, Izumi Watanabe, and Katsuji Kuno. 2004. "Investigation of the Heavy Metal Sources in Relation to Automobiles." Water, Air, & Soil Pollution, 157 (1–4), 209–223.

Panko, Julie, Kristen Hitchcock, Gary Fuller, and David Green. 2019. "Evaluation of Tire Wear Contribution to $PM_{2.5}$ in Urban Environments." Atmosphere, 10 (2), 99.

Panko, Julie, Marisa Kreider, and Kenneth Unice. 2018. "Review of Tire Wear Emissions. In: Non-Exhaust Emissions." Elsevier, 147–160.

Panko, Julie M., Jennifer Chu, Marisa L. Kreider, and Ken M. Unice. 2013. "Measurement of airborne concentrations of tire and road wear particles in urban and rural areas of France, Japan, and the United States." Atmospheric Environment, 72, 192–199.

Park, Inyong, Hongsuk Kim, and Seokhwan Lee. 2018. "Characteristics of tire wear particles generated in a laboratory simulation of tire/road contact conditions." Journal of Aerosol Science, 124, 30–40.

Piscitello, Amelia, Carlo Bianco, Alessandro Casasso, and Rajandrea Sethi. 2021. "Non-exhaust traffic emissions: Sources, characterization, and mitigation measures." Science of The Total Environment, 766, 144440.

Pohrt, Roman. 2019. "Tire Wear Particle Hot Spots – Review of Influencing Factors." Facta Universitatis, Series: Mechanical Engineering, 17 (1), 17.

Prenner, Stefanie, Astrid Allesch, Margarethe Staudner, Martin Rexeis, Michael Schwingshackl, Marion Huber-Humer, Florian Part. 2021. "Static modelling of the material flows of micro- and nanoplastic particles caused by the use of vehicle tyres." Environmental Pollution, 290, 118102.

Rauterberg-Wulff, Annette. 1999. "Determination of emission factors for tire wear particles by tunnel measurements. In: 8th International Symposium" Transport and Air Pollution," June 1999 Graz, Austria.

Reddy, Christopher M., and James G. Quinn. 1997. "Environmental Chemistry of Benzothiazoles Derived from Rubber." Environmental Science & Technology, 31 (10), 2847–2853.

Rhodes, Emily P., Zhiyong Ren, and David C. Mays. 2012. "Zinc Leaching from Tire Crumb Rubber." Environmental Science & Technology, 46 (23), 12856–12863.

Rogge, Wolfgang F., Lynn M. Hildemann, Monica A. Mazurek, Glen R. Cass, and Bernd R. T. Simoneit. 1993. “Sources of fine organic aerosol. 3. Road dust, tire debris, and organometallic brake lining dust: roads as sources and sinks.” Environmental Science & Technology, 27 (9), 1892–1904.

Saito, Takashi. 1989. “Determination of styrene-butadiene and isoprene tire tread rubbers in piled particulate matter.” Journal of Analytical and Applied Pyrolysis, 15, 227–235.

Salminen, Henry, 2014. “Parametrizing tyre wear using a brush tyre model.” Student thesis. TRITA-AVE.

Sjödin, Åke, Martin Ferm, Anders Björk, Magnus Rahmberg, Anders Gudmundsson, Erik Swietlicki, Christer Johansson, Mats Gustafsson, Göran Blomqvist. 2010. “Wear particles from road traffic-a field, laboratory and modelling study.” Final report. IVL Svenska Miljöinstitutet.

Snilsberg, Brynhild., 2008. “Pavement wear and airborne dust pollution in Norway.”

Spies, Robert B., Brian D. Andresen, and David W. Rice. 1987. “Benzthiazoles in estuarine sediments as indicators of street runoff.” Nature, 327 (6124), 697–699.

Sun, Jian, Steven Sai Hang Ho, Xinyi Niu, Hongmei Xu, Linli Qu, Zhenxing Shen, Junji Cao, Hsiao-Chi Chuang, and Kin-Fai Ho. 2022. “Explorations of tire and road wear microplastics in road dust $PM_{2.5}$ at eight megacities in China.” Science of The Total Environment, 823, 153717.

Thorpe, Alistair, Roy M. Harrison, 2008. “Sources and properties of non-exhaust particulate matter from road traffic: A review.” Science of The Total Environment, 400 (1–3), 270–282.

Tonegawa, Yoshio, and Sousuke Sasaki. 2021. “Development of Tire-Wear Particle Emission Measurements for Passenger Vehicles.” Emission Control Science and Technology, 7 (1), 56–62.

Unice, Kenneth M., Jennifer L. Bare, Marisa L. Kreider, and Julie M. Panko. 2015. “Experimental methodology for assessing the environmental fate of organic chemicals in polymer matrices using column leaching studies and OECD 308 water/sediment systems: Application to tire and road wear particles.” Science of The Total Environment, 533, 476–487.

Unice, Kenneth M., Marisa L. Kreider, and Julie M. Panko. 2012. “Use of a Deuterated Internal Standard with Pyrolysis-GC/MS Dimeric Marker Analysis to Quantify Tire Tread Particles in the Environment.” International Journal of Environmental Research and Public Health, 9 (11), 4033–4055.

USEPA, 2020. “Brake and Tire Wear Emissions from Onroad Vehicles in MOVES3.” Assessment and Standards Division, Office of Transportation and Air Quality, U.S. Environmental Protection Agency, No. EPA-420-R-20-014.

Veith, A.G., 1973. “Accelerated Tire Wear under Controlled Conditions. II. Some Factors that Influence Tire Wear.” Rubber Chemistry and Technology, 46 (4), 821–842.

Wagner, Stephan, Thorsten Hüffer, Philipp Klöckner, Maren Wehrhahn, Thilo Hofmann, and Thorsten Reemtsma. 2018. “Tire wear particles in the aquatic environment—A review on generation, analysis, occurrence, fate and effects.” Water Research, 139, 83–100.

Weckwerth, Gerd. 2001. “Verification of traffic emitted aerosol components in the ambient air of Cologne (Germany).” Atmospheric Environment, 35 (32), 5525–5536.

Wik, Anna, and Göran Dave. 2009. “Occurrence and effects of tire wear particles in the environment – A critical review and an initial risk assessment.” Environmental Pollution, 157 (1), 1–11.

Appendix

A Literature Review on Tire-wear Particulate Matter Emissions

Introduction

Tire-wear emissions directly result from the interaction between a pavement surface and tires. The shear and slip forces caused by the contact of the tires and the thermochemical degradation of the tires are the main causes of particle generation (Denier van der Gon et al. 2013, Grigoratos and Martini 2014, Klüppel 2014, Wagner et al. 2018, Panko et al. 2019).

Direct measurements of tire wear was achieved by the periodic measurement of tread depth or the measurement of tire weight. Monitoring the generation of tire-wear particles is often done by monitoring the mean of a tire's mass distribution, with most researchers reporting a unimodal or bimodal distribution shape of the particle-size distribution. However, tire-wear emissions are often estimated using emission factors. Emission factors either average the number of emissions each vehicle generated after covering a certain unit distance or sum up the weight of the particles by multiplying the weight loss of each tire by the number of tires (Denier van der Gon et al. 2013, Baensch-Baltruschat et al. 2020, EPA 2020, Piscitello et al. 2021).

Studies focusing on investigating tire-wear emissions have been conducted both in the field and laboratory environments. Prominent methods were divided into five categories (Grigoratos and Martini 2014, Wagner et al. 2018):

- Active vehicle measurements: a device able to capture emissions levels is installed in a vehicle. Testing is usually conducted under ambient conditions (Gehrig et al. 2010, Oroumiyeh and Zhu 2021)
- Tire-wear tracers (Alexandrova et al. 2007, Keuken et al. 2010)
- Source apportionment methods (Luhana et al. 2004, Amato et al. 2016, Oroumiyeh et al. 2022)
- Laboratory road simulators (Gustafsson et al. 2012, Park et al. 2018)
- Generating tire wear in a laboratory by abrasion (e.g., steel brush) (Kreider et al. 2010)

The contribution of non-exhaust emissions to total traffic emissions has risen to be almost equal to that of exhaust emissions in recent years due to improved fuel efficiency, regulations, and standards imposed by the EPA and other regulating organizations as well as by the increasing percentage of electric vehicles (Oroumiyeh and Zhu 2021). Tire-wear emissions, despite only being a portion of non-tailpipe emissions, can contribute up to 10 percent of the ambient PM_{10} (Panko et al. 2018).

Factors Affecting the Generation and Particle Distribution of Tire Wear

Influence of Pavement Surface

Influence of Pavement Type and Mixture Properties

Gustafsson et al. (2012) studied the effect of some of the asphalt concrete pavement and mixture properties, like the maximum aggregate size and the aggregate properties, in Sweden. The study evaluated emissions on a pavement surfaced with stone mastic asphalt (SMA). The study also benchmarked the results against different types of pavements, including asphalt rubber, open-graded porous asphalt, and concrete pavements. The investigation was conducted both in a laboratory and in the field. Lab measurements were done using a road simulator, as shown in Figure 43. In the field, direct PM_{10} emissions were measured in stationary locations utilizing vans equipped with real-time aerosol sensors that measure the difference between the emissions from the van's front and rear tires to determine the particle emissions generated due to tire wear.

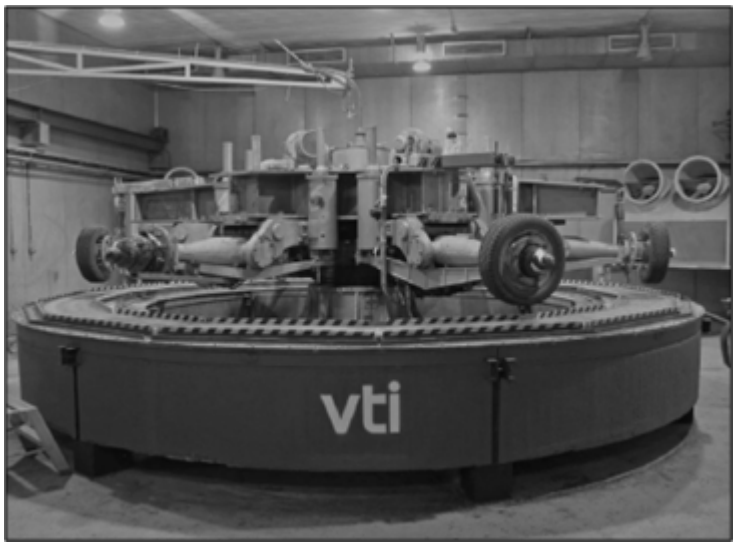

Figure 43. VTI Road Simulator (Gustafsson et al. 2012)

The study showed that maximum aggregate size had a direct correlation with PM_{10} emissions, as the emissions increased with the smaller maximum size. No conclusions could be made about the correlation of Los Angeles abrasion values, obtained from a test used to measure aggregates resistance to degradation, of the aggregates used in the study and the observed emissions. The authors attributed the lack of correlation to the fact that all the aggregates used in the study had somewhat similar values. However, they referred to earlier work by the Swedish Cement and Concrete Research Institute, where the higher abrasion values were shown to lead to higher emissions. Gustafsson et al. (2015) showed that although a concrete surface can be more resistant to abrasion and wear, the concrete pavement had higher PM_{10} emissions mainly due to the calcium particles generated from the surface wear.

The variance between the different types of pavements was evaluated while using SMA pavements as a point of reference. The open-graded porous pavements exhibited lower emissions values in the road simulator due to wear-resistant aggregates, while the field study showed comparable values to SMA. The concrete pavements consistently generated lower emissions in both lab and field studies, with a reduction ranging between 19 and 28 percent. Finally, the measurements from asphalt rubber yielded 20–25 percent fewer emissions when compared to the reference measurements.

In a study that compared surface wear of asphalt and concrete pavements in Houston, TX, the asphalt surface was reported to result in a slightly higher tire-wear emission than concrete-surfaced pavement. However, the rate of surface wear was higher in the concrete pavement (Fiala and Hwang 2021).

An Arizona study compared tire-wear emissions from asphalt rubber and concrete pavements. The study worked to identify tire-wear tracer compounds using composite tire-wear samples. Extraction and separation of aerosol samples were then employed to measure the tire-wear emission rate. The concrete pavements were found to produce almost 1.4–2.0 times the tire-wear emissions emitted by rubberized asphalt surfaces (Allen et al. 2006, Alexandrova et al. 2007).

Pohrt (2019) reported an inversely proportional relationship between asphalt mixture density and tire wear.

Influence of Pavement Condition

Barlow (2014) highlighted the effect of pavement condition on tire wear. An increase in pavement friction was expected to lead to higher tire wear. Distresses in the pavement section, like potholes and cracks, were also expected to lead to higher tire-wear emissions.

Lowne (1970) reported that increased surface harshness (microtexture) had a direct correlation with tire-wear rate when in contact with the asphalt surface, while roughness (macrotexture) had less of an effect based on tire-loss measurements.

Temporal and Spatial Variations

Weather and climatic variations can have significant impact on tire-wear emissions over various time span of a day or a season. In particular, temperature, humidity, wind speed and direction, and whether the surface is in wet or dry condition are among the climatic factors affecting tire wear. Rainy events accumulate moisture on the road surface that can lead to less friction and a lower degree of wear. Similarly, higher relative humidity leads to a reduction in airborne tire-wear particles (Johansson et al. 2007, Keuken et al. 2010). The ambient temperature and that of the pavement surface are directly proportional to the tire temperature and wear (Veith 1973, Klüppel 2014, EPA 2020). For this same reason, wind velocity affects tire-wear emissions since lower wind velocities lead to lower tire temperatures (Veith 1973).

Vehicle Characteristics

Weight

Heavier vehicles lead to higher tire wear and tire-wear emissions (Luhana et al. 2004, Pohrt 2019, Amato et al. 2020, EPA 2020, Harrison et al. 2021, Oroumiyeh and Zhu 2021). EPA MOVES factors the influence of vehicle weight on tire-wear emissions by accounting for higher emissions based on the number of tires on each vehicle (EPA 2020).

Oroumiyeh and Zhu (2021) studied the tire wear of three different types of vehicles in California. The study found that heavier vehicles emit both PM_{10} and $PM_{2.5}$ at significantly higher levels than smaller vehicles.

Most other studies on the influence of vehicle weight were done in a laboratory environment. While all studies agree on the positive correlation between the tire wear and the weight of the vehicles, the nature of the relationship is still not clear. For instance, Pohrt (2019) found the relationship between tire wear and weight to be linear, while Salminen (2014) suggested the tire-wear rate increases exponentially with the increase in the vehicle weight (Amato et al. 2020). Beddows and Harrison (2021) derived the relationship between vehicle weight and tire wear based on the emission factors recommended by the United Kingdom's Air Quality Expert Group, and their findings appear to be more in line with those of Amato et al. (2020), as shown in Figure 44.

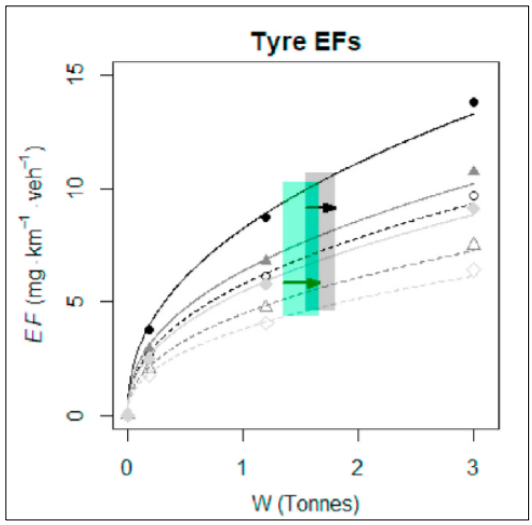

Figure 44. Relationship Between Vehicle Weight and Tire Wear (Beddows and Harrison 2021)

Suspension

The effect of a vehicle suspension system on tire wear could be attributed to two design factors: the camber angle and the toe angle. The camber angle is the angle between the XZ plane of the wheel and a line perpendicular to the plane of pavement on the YZ plane of the vehicle. A higher camber angle would reduce tire wear, but it would have a negative impact on the tire's gripping and handling.

The toe angle is the angle between the XZ plane of the wheel and the XZ plane of the vehicle. A smaller toe angle would reduce tire wear (Goodarzi and Khajepour 2017). Figure 45 and Figure 46 highlight the difference between the two angles.

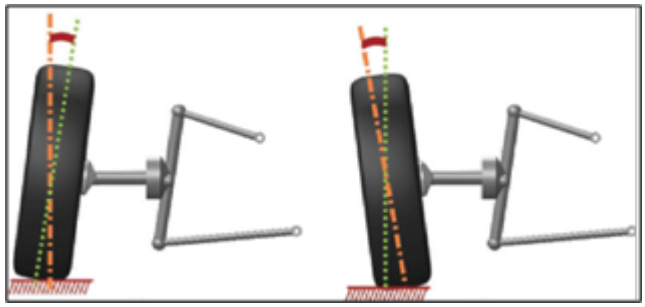

Figure 45. Camber Angle in a Vehicle Suspension System (Goodarzi and Khajepour 2017)

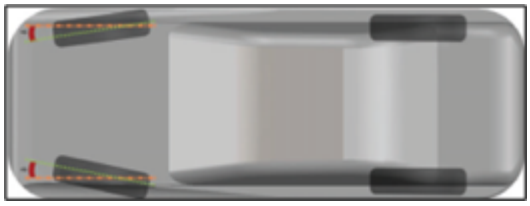

Figure 46. Toe Angle in a Vehicle Suspension System (Goodarzi and Khajepour 2017)

Axles and Steering Geometry

Tires that are subjected to a larger slip angle wear faster. When small radius turns are performed, tires on vehicles with multiple axles often generate very high slip angles. Additionally, the lateral slip angle increases with the distance between the axle and effective axle position for unsteerable axles. Therefore, the geometry could be the primary factor affecting tire wear for larger vehicles (Lepine et al. 2021).

Traffic Pattern

Driving Speed

Luhana et al. (2004) evaluated the effect of the speed of five types of light weight vehicles on tire wear after two months of operation in several types of streets. The wear rate of light vehicles on highways ranged between 56 mg and 67 mg TWRP.km^{-1}.veh^{-1} (0.0032 oz and 0.0038 oz TWRP.mile^{-1}.veh^{-1}), while the rate of those driven on suburban and rural streets averaged around 85 mg TWRP.km^{-1}.veh^{-1} (0.0048 oz TWRP.mile^{-1}.veh^{-1}), which indicates higher speed leads to lower tire wear (EPA 2020). Based on the findings of this study, the EPA's MOVES primarily uses speed to estimate the tire-wear emissions while factoring in vehicle weight.

Despite the findings of Luhana et al. (2004), most other studies suggest that higher driving speed led to higher tire wear and higher tire-wear emissions with finer particles (Snilsberg 2008, Salminen 2014, Grigoratos et al. 2018, Kim and Lee 2018, Amato et al. 2020). Kim and Lee (2018) noticed an increase in PM_{10} and $PM_{2.5}$ tire-wear emissions and a $PM_{2.5}/PM_{10}$ ratio in a tire simulator when they gradually

increased the speed under a steady lateral load. Similarly, when they kept the vehicle speed constant and increased the lateral load, both PM_{10} and $PM_{2.5}$ increased. They also noted a dramatic increase in tire-wear-emission generation when slip speed increased in a tire simulator.

Tonegawa and Sasaki (2021) found that there is no significant change in tire-wear emissions when vehicle speed is between 20–40 km/hr [12.4–24.8 mph]. However, lateral acceleration had a significant impact on tire wear and emissions.

Traffic Volume

In a study comparing road-dust emissions in 20 locations in Philadelphia, PA, O'Shea et al. (2020) found that areas with the largest traffic volume had significantly higher mean organic concentrations due to tire wear. However, other researchers found that traffic count had no significant impact on the rate of tire-wear emissions (Panko et al. 2019, Knight et al. 2020).

Acceleration and Breaking Events

Tire wear increases when the vehicle is accelerating and during braking (EPA 2020). Recently, several researchers identified braking and accelerating as the factors that have the highest influence on tire-wear emissions (Knight et al. 2020). Oroumiyeh and Zhu (2021) showed that when the braking intensity increases, so do the tire-wear $PM_{2.5}$ and PM_{10} emissions. Kim and Lee (2018) found a dramatic increase in tire-wear emissions when they brought a tire simulator operating at 130 km/hr [80.8 mph] to a full stop within one minute.

Tire-wear Markers

Tire-wear Components (Tire Composition)

Rubber from model passenger car tires consists of approximately six major components (Wik and Dave 2009):

- rubber polymer (40–60 percent)
- reinforcing agent/filler (20–35 percent)
- process oils (15–20 percent)
- vulcanization system (4 percent)
- protective agents (1 percent)
- processing aids (<1 percent)

The rubber polymers often contain a blend of natural rubber compounds (isoprene (2-methyl butadiene)) and synthetic petroleum-based rubbers (polyisoprene, polybutadiene, or styrene-butadiene (SBR)) (Wagner et al. 2018). Of the total global rubber usage, natural rubber accounts for 35 percent of global composition, SBR for 18 percent, and other synthetic rubbers, such as polybutadiene, make up the remaining 47 percent (Barbin and Rodgers 1994), with SBR being the most commonly used rubber polymer in passenger car tires (Wagner et al. 2018).

Reinforcing agents/fillers are used to improve the rubber's strength characteristics in terms of hardness and wear resistance, with the most common filler being carbon black, followed by other materials such as silica with a silane coupling agent and a carbon-silica dual phase (Grigoratos and Martini 2014). In the past, process oils consisted of high-aromatic oils such as mineral oil, which contained a high content of polycyclic aromatic hydrocarbons (PAHs); however, due to the toxicity of PAHs, they have become more regulated, leading to an increased use of mild extract solvates and treated distillate aromatic extracts as alternative oils (Wik and Dave, 2009). The vulcanization system is used to crosslink polymer chains within the rubber to improve its physical characteristics and typically contains (Barbin and Rodgers 1994, Wik and Dave 2009):

- activators (zinc oxide and stearic acid)
- vulcanizing agents (sulfur, insoluble sulfur, and peroxides)
- accelerators (N-Oxydiethylene benzothiazole-2-sulfenamide (OBS), N-Cyclohexyl-2-benzothiazole sulfenamide (CBS), aldehydeamines, thioureas, guanidines, thiazoles, sulfenamides, dithiocarbamates, thiurams, and xanthates)
- retarders (N-cyclohexylthiophthalimide, benzoic acid, and N-nitrosodiphenylamine)

A wide range of protective agents are used to prevent degradation of the rubber, including (Barbin and Rodgers 1994):

- diamines
- phosphites
- waxes
- hydroquinones
- phenols
- para-phenylenediamines

Processing aides can include (Barbin and Rodgers 1994, Wik and Dave 2009):

- plasticizers (esters, pine tars, and low-molecular-weight polyethylene)
- peptizers (pentachlorothiophenol, phenylhydrazine, diphenylsulfides, and xylyl mercaptan)
- preservatives (halogenated cyanoalkanes)
- desiccants (calcium oxides)

Criteria for Ideal Tire-wear Marker

Wagner et al. (2018) detailed the key criteria to consider when identifying a marker to be used in tire-wear analysis. The marker should:

1. be present in all tire materials in comparable portions largely independent from manufacturer/process
2. not leach easily from tire particles into the surrounding environment
3. not be easily transformed while the particles reside in the environment

4. be sufficiently specific for tires
5. have a concentration in tire material significantly higher than in particles forming the sample matrix
6. be analytically accessible by methods of high precision, accuracy, and sensitivity

Rubber as a Tire-wear Marker

While rubber is the main constituent of tires, it is a polymer of high molecular weight, making it difficult to study via chemical analyses. Instead, one must use pyrolysis to generate rubber-specific volatile breakdown products which then can be analyzed (Wagner et al. 2018). SBR is a common rubber component used as a tire-wear marker for air and soil samples where the pyrolysis products of styrene, butadiene, and vinylcyclohexene are the components being detected (Cadle and Williams 1978, Lee et al. 1989, Saito 1989, Unice et al. 2012, Panko et al. 2013, 2019, Sun et al. 2022). In addition to SBR, natural rubber and butadiene rubber were also quantified by their pyrolysis products: isoprene and dipentene for natural rubber, and butadiene and vinylcyclohexene for butadiene rubber (Lee et al. 1989, Saito 1989, Unice et al. 2012, Panko et al. 2013, 2019, Sun et al. 2022). SBR was also quantified without the need for pyrolysis using infrared spectroscopy (Fauser 1999).

Benzothiazoles as Tire-wear Markers

Although vulcanization accelerators (benzothiazoles) only account for 0.5 percent of tire material, many studies have used these additives to quantify tire wear in the environment, as a substantial amount of these compounds originate only from rubber. The most commonly used benzothiazoles are 2-(4-morpholinyl) benzothiazole (24MoBT), originating from the OBS accelerator, and N-cyclohexyl-2-benzothizaolamine (NCBA) from the CBS accelerator (Wagner et al. 2018). Spies et al. (1987) was able to quantify 24MoBT, benzothiazole, and 2-methylmercapto-benzothiazole in sediment from the San Francisco Bay, concluding that it indicated the contribution of street runoff to sediment contaminants. They also analyzed Delac™ MOR©, a commercial product used in tire manufacturing, and found that the major component was 2-(morpholinothio)-benzothizaole, with a degradation product of benzothiazole (BT), and impurities of 24MoBT and 2-methylmercapto-benzothiazole. Kim et al. (1990) analyzed tire tread samples in addition to suspended PM (PM). They found that BT was common to all classes of tire tread tested and is suitable for the quantitative determination of tire tread in suspended PM. Rogge et al. (1993) also quantified BT in environmental samples, detecting it in resuspended road rust and tire-debris particles, but not brake-wear PM.

Kumata et al. (1996) developed a method for quantifying 24MoBT in environmental samples such as street dust, aerosols, and sediments. Building off of this work, they were able to quantify 24MoBT and NCBA in street runoff, asphalt leach samples, antifreeze samples, sediment, road dust, and atmospheric aerosols (Kumata et al. 2000, 2002). While they found significant amounts of 24MoBT and NCBA in the antifreeze samples, it was still substantially smaller than the contribution from tire particles, and no 24MoBT or NCBA were detected in the asphalt samples (Kumata et al. 2002). Reddy and Quinn (1997) also quantified BT, 24MoBT, 2-hydroxybenzothiazole (HOBT) and 2-methylbenzothiazole (MeBT) in crumb rubber material (CRM), antifreeze, urban runoff, pond water, sediment, road dust, and urban PM.

As expected, significant amounts of BT, HOBT, and 24MoBT were present in the CRM and present in much smaller quantities in the antifreeze samples tested, while all three were detected in urban runoff, settling-pond water, urban PM, road dust, and sediments. Alexandrova et al. (2007) also tested for the presence of 24MoBT and NCBA in aerosols, tire-tread samples, and CRM. While they were able to quantify 24MoBT in the CRM sample, they were unable to quantify 24MoBT or NCBA in their aerosol samples from the tunnel study conducted in Arizona. Instead, they quantified two species containing benzothiazole and benzothiazolesulfenamide moieties in aerosol samples and tire tread samples; however, the study did not properly identify these species.

Avagyan et al. (2014) analyzed urban PM, asphalt, and tire samples for a variety of vulcanization accelerators including BT, 2-mercaptobenzothiazole (MBT), 2,2'-dithiobisbenzothiazole (MBTS), 2-methylthio benzothiazole (MTBT), and N-cyclohexyl-2-benzothiazole sulphenamide (CBS). All five compounds were quantified in the various tire samples tested, while only BT was quantified in the asphalt sample. In both the PM_{10} and total suspended particulate aerosol samples, all five were detected, but only MBT and BT were quantifiable. Knight et al. (2020) used NCBA as a marker for tire wear present in wet sediment samples, and were able to detect its presence in half of the samples they analyzed.

The downsides to using benzothiazoles as tire-wear markers are that the primary benzothiazoles used in rubber manufacturing are often transformed into other benzothiazole moieties during the rubber-curing process and organic extractions may require relatively harsh conditions or clean-up procedures (Wagner et al. 2018).

Other Potential Tire-wear Markers

Zinc has also been used as a tire-wear marker as it is used in the form of zinc oxide as a vulcanization activator and as organozinc compounds (Zinc dibutyldithiocarbamate, Zinc dimethylthiocarbamate) as vulcanization accelerators (Barbin and Rodgers 1994). Rhodes et al. (2012) demonstrated that zinc leaches into the environment from tire crumb rubber, while Councell et al. (2004) estimated the amount of zinc released to the environment from tire wear. Fauser (1999) developed a method to quantify the extractable organic zinc present in aerosol and soil samples. Unice et al. (2012) also developed a method to measure organic zinc in soil samples, but they did not continue the work as the organic zinc recovery from the soil extraction was too low. Kreider et al. (2010) was able to measure elemental zinc in tire-wear particles, roadway particles, and tread samples, finding that the amount of zinc in the tread samples was two to three times more than the tire-wear and roadway samples, indicating tire treads as a major contributor of zinc in these samples. However, there are other anthropogenic sources of zinc, such as gasoline combustion (Weckwerth 2001), diesel soot, and peeled guardrail paints (Ozaki et al. 2004) that would further complicate the use of zinc as a tire-wear marker. The benefit of using extractable organic zinc as a tire-wear marker is that the only interfering factor is spilled engine oil (Fauser 1999).

Additional proposed tire-wear markers include PAHs and aliphatic hydrocarbons; however, these are also found in asphalt, automobile exhausts, and fuel combustion products, while resin acids (dehydroabietic acid) have natural sources (Wagner et al. 2018). Newer proposed markers for tire wear

are the vulcanization agent 1,3-diphenylguanidine (DPG) and the antioxidant (N-(1,3-dimethylbutyl)-N'-phenyl-1,4-phenylenediamine (6-PPD)) (Unice et al. 2015). These compounds were found to be more stable during the rubber-curing process and less prone to leach than benzothiazoles, but more research is needed regarding their prevalence in aerosols.

Tire-wear Chemical Analyses

Mass Spectrometry

This section will discuss multiple types of mass spectrometry analysis, meaning the analyses all use differences in mass-to-charge ratios (m/z) to identify and quantify the analytes of interest. The distinction between these analyses is the sample-introduction and ion-source methodologies.

Inductively Coupled Plasma Mass Spectrometry

ICP–MS is primarily used for elemental analysis, where the ICP serves as both the sample inlet and ionization source. With this technique, one can detect almost 80 elements on the periodic table with detection limits much lower than conventional emission spectroscopy. ICP–MS has been used by several researchers studying elemental zinc that has been leached into the environment from tire material. Unice et al. (2012) were able to extract inorganic zinc from artificial soil spiked with synthetic tire-tread particulates and quantified the zinc content with ICP–MS. Rhodes et al. (2012) used ICP–MS to measure the amount of zinc that was leached from crumb rubber tire material.

High Pressure Liquid Chromatography –Mass Spectrometry

High pressure liquid chromatography–mass spectrometry (LC–MS) is used on compounds with high molecular mass that are involatile and/or polar. The liquid chromatograph portion of the instrument is used to separate the sample into its components, often by their polarity, prior to entering the mass spectrometer. This leads to better specificity and lower limits of detection for individual analytes. In some instances, tandem mass spectrometry (LC–MS/MS) is used to achieve even higher specificity and lower detection limits. It can also allow for structural elucidation of the target analytes.

Avagyan et al. (2013) developed a LC–MS/MS method to quantify benzothiazole (BT), 2-mercaptobenzothiazole (MBT), 2,2'-dithiobisbenzothiazole (MBTS), 2-methylthiobenzothiazole (MTBT), and N-cyclohexyl-2-benzothiazole sulphenamide (CBS) in tire rubber samples. This same method was also used to quantify BT, MBT, MBTS, MTBT, and CBS in urban PM, asphalt, and tire samples (Avagyan et al., 2014).

Unice at al. (2015) also used a LC–MS/MS technique to quantify BT, MBT, CBS, MBTS, 2-methylbenzothiazole (MeBT), N-cyclohexyl-1,3-benzothiazol-2-amine (NCBA), and other possible transformation products of CBS from tire- and road-wear particles in soil samples. Barnes et al. (2003) used LC–MS to search for traces of BT, MBT, MBTS, and CBS in food and drink that came into contact with rubber, however did not find any trace in the tested samples.

Gas Chromatography–Mass Spectrometry

Gas chromatography–mass spectrometry (GC–MS) is a widely used analytical technique for identifying and quantifying volatile compounds with molecular masses less than ~600 Daltons, sometimes up to 1000 Daltons depending on the instrument setup. The gas chromatograph instrument first separates components of the sample as a function of their polarity and volatility. As with LC–MS, these components then enter the mass spectrometer where they are separated by their m/z and quantified. Spies et al. (1987) used GC–MS to quantify benzothiazole components (24MoBT, BT, and 2-methylmercapto-benzothiazole) of Delac MOR, a commercial tire manufacturing product, and used their results to identify evidence of tire-wear particles in sediment samples. Compared to the LC–MS/MS method used by Avagyan et al. (2013), the GC–MS method resulted in a limit of detection approximately 50 times higher for BT.

Rogge et al. (1993) were able to quantify a large variety of organic species, including BT, in resuspended road dust, tire-debris PM, and brake-wear PM using GC–MS.

Reddy and Quinn (1997) analyzed CRM, antifreeze, urban runoff, pond water, sediment, road dust, and urban PM for BT, 24MoBT, MeBT, and 2-hydroxybenzothiazole (HOBT) using GC–MS and a variety of extraction steps.

Alexandrova et al. (2007) also used GC–MS to study 24MoBT and NCBA in aerosols, tire-tread samples, and CRM. However, to properly isolate the analytes of interest, they first had to extract the organic components using a Soxhlet extraction, ultrasonic extraction, and acid extraction followed by a concentrating step, which was first described in Kumata et al. 1996. Kumata et al. (2000) modified this method to include PAHs and alkylbenzenes; this method was used in Knight et al. (2020) to measure NCBA in wet sediment samples to quantify tire wear.

Franklin et al. (2021) used a more uncommon method of GC/GC–MS to cover compounds of differing volatility ranges to quantify benzothiazole compounds originating from sea spray aerosols.

One downside of using GC–MS to quantify benzothiazoles is the tendency for BT derivatives to thermally degrade into BT or MBT, giving information on total quantity of BT rather than individual components (Barnes et al. 2003).

GC–MS has also been used to measure the natural rubber, SBR, and butadiene rubber (BR) content of samples by pyrolyzing the samples prior to GC–MS analysis (pyr-GC–MS). This pyrolysis produces characteristically smaller fragments that the GC–MS can analyze more easily than the larger rubber polymers. Unice et al. (2012) developed a pyr-GC–MS method using deuterated internal standards to quantify the fragmentation products of NR, SBR, and BR (isoprene, butadiene, styrene, vinylcyclohexene, and dipentene isomers).

Panko et al. (2013, 2019) used this method to determine the concentration of tire- and road-wear particles in air samples by quantifying 4-vinylcyclohexene and dipentene. Lee et al. (2007) used pyr-GC–MS to analyze blends of NR, SBR, and BR using the fragmentation products of isoprene, butadiene, styrene, vinylcyclohexene, dipentene, and 1-methyl-4-(1-methylethenyl)-cyclohexene to identify the specific rubber composition.

Sun et al. (2022) quantified NR, SBR, and BR in urban PM samples using pyr-GC–MS.

Gas Chromatography

Gas chromatography without mass spectrometry has also been used to quantify benzothiazoles and rubber pyrolysis products. Kumata et al. (1996) developed a gas chromatography method using a flame photometric detector (GC-FPD) to quantify 24MoBT in environmental samples. FPD is particularly sensitive to sulfur-containing compounds such as benzothiazoles and works by passing the sample through a flame and measuring the light emitted from the compound. Kumata et al. (1996, 2002) used this method to measure 24MoBT and NCBA in road dust, runoff water, river sediment, and asphalt samples. Kim et al. (1990) and Cadle and Williams (1978) also used GC-FPD to analyze sulfur-containing compounds (thiophene, 2-methylthiopene, 3-methylthiopene, and benzothiazole) in tread rubber, aerosols, and soil samples. The use of GC-FPD for benzothiazole quantification has fallen out of favor with recent developments in mass spectrometry technologies.

Prior to advancements in mass spectrometry, gas chromatography with a flame ionization detector (GC-FID) was the primary method of analyzing the rubber content of samples. FID is one of the most-used detectors on GC systems as it is more mass-sensitive than concentration-sensitive and is insensitive toward water and common atmospheric gases. It works by passing the sample through a flame and detecting the current produced by the analytes as they pyrolyze. Both Lee et al. (1989) and Saito (1989) developed pyr-GC-FID methods to quantify the amount of NR and SBR in atmospheric dust and tire-tread samples, respectively. Kim et al. (1990) and Cadle and Williams (1978) also used pyr-GC-FID to determine levels of NR, SBR, and BR (vinylcyclohexene, dipentene, and styrene) in tire-tread and suspended PM samples.

Miscellaneous Other Methods

In addition to ICP–MS, several other techniques have been used to measure zinc in the tire wear present in environmental samples. Kreider et al. (2010) used inductively coupled plasma atomic emission spectroscopy (ICP-AES) after microwave-assisted acid digestion to quantify zinc in tire-wear particles, roadway particles, and tire-tread samples. ICP-AES has a similar sample ionization step as ICP–MS, but instead of passing the ions to a mass spectrometer detector, ICP-AES detects the emission spectra of ions in the sample using an optical spectrometer. Callender and Rice (2000) also used ICP-AES to study anthropogenic zinc present in sediment samples.

Another spectroscopic technique for measuring zinc is atomic absorbance spectroscopy (AAS). Ozaki et al. (2004) used AAS to measure the zinc content in fuel sources, road dust, traffic paint, asphalt, exhaust soot, soil, and guardrail paint. With AAS, the sample is atomized and then passed through a radiation source, and the absorption at specific wavelengths is measured to determine elemental concentration.

Fauser (1999) also used AAS with two different atomizers (flame atomic absorbance spectroscopy and heated graphite atomizer (HGA)) to determine the concentration of zinc in aerosol and soil samples. Weckwerth (2001) used instrumental neutron activation analysis (INAA) to study the heavy metal content, which includes zinc, of aerosols. INAA works by bombarding the sample with neutrons and measuring the characteristic gamma rays emitted from the heavy metal atoms.

Infrared spectroscopy (IR) has been used to determine the SBR, NR, and BR concentrations in a variety of samples. Lee et al. (2007) used Fourier-transform infrared spectroscopy (FT-IR) on pyrolyzed rubber samples to determine their specific SBR, NR, and BR composition. With FT-IR, the sample is exposed to infrared radiation, and the resulting absorption is measured. The resulting spectra contain information about the vibrational and rotational states of the analyte, which is useful for qualitative analysis of organic species. Fauser (1999) used an extraction step prior to FT-IR analysis to quantify the SBR content of tire, asphalt, engine oil, aerosol, and soil samples. However, Fauser's FT-IR method has a tire material limit of detection 1.5 times higher than the HGA method.

Another method for measuring rubber content in environmental samples is thermogravimetric analysis (TGA), where the mass of the sample is monitored as the temperature increases. This can be used to measure the thermal stability of a polymer or the thermal degradation of polymer blends. Lee et al. (2007) used TGA and differential scanning calorimetry (DSC) to determine the blend composition of samples containing NR, SBR, and BR. DSC measures the heat flow differences between the sample and a reference and is used to characterize the thermal degradation of elastomers. Cadle and Williams (1978) also used TGA to determine the oil, polymer, and carbon black content of tire treads in PM samples, while (Unice et al. 2015) used TGA to quantify the polymer content in tire-tread samples.